Q. J. R. Meteorol. Soc. (2000), **126**, pp. 3255–3286

Internal wave reflection in uniform shear

By B. R. SUTHERLAND*
University of Alberta, Canada

(Received 19 November 1999; revised 27 April 2000)

SUMMARY

If nonhydrostatic internal waves are of sufficiently large amplitude, they undergo significant dispersion due to interactions between the waves and wave-induced mean flow. The effect of these interactions is investigated for internal waves propagating upward in a uniformly stratified Boussinesq flow with uniform shear. The sign of the shear is established so that the wave intrinsic frequency increases as the wave packet propagates upward; hence linear theory predicts that the waves should reflect at some level. Fully nonlinear numerical simulations of two-dimensional wave packets are performed to study the wave-packet evolution as a function of the initial amplitude and spatial extent of the wave packet. It is shown that if the waves are horizontally periodic, and of sufficiently large amplitude, momentum is permanently deposited to the mean flow at altitudes near, but below, the reflecting level predicted by linear theory. If the waves are horizontally compact, the waves propagate upward well above the reflection level.

KEYWORDS: Gravity-wave drag Reflection level Stability

1. INTRODUCTION

Linear theory is often employed to estimate how momentum and energy are redistributed in the atmosphere and ocean by internal waves. Provided the waves are of sufficiently small amplitude and if the background stratification and mean flow speed vary sufficiently gradually with height, the path of an internal wave packet is well predicted. In particular, if a two-dimensional internal wave packet propagates upward in uniformly stratified fluid with uniform shear, linear theory predicts that one of three things will happen. The waves may approach a critical level, where the horizontal phase speed of the waves equals the background flow speed. In this case the waves asymptotically approach the critical level and eventually break or dissipate thus depositing momentum to the mean flow. If the shear is of opposite sign, the waves may approach a reflecting level, where the Doppler-shifted frequency of the waves equals the background buoyancy frequency. In such circumstances the momentum and energy fluxes are redirected back toward the wave source. In the atmosphere a third possibility exists: due to anelastic (non-Boussinesq) effects waves may grow to sufficiently large amplitude, as they propagate upward into the less dense atmosphere, that they overturn and break. (For further discussion, see Bretherton (1966), Booker and Bretherton (1967), Bretherton (1969), Lighthill (1978) section 4.6, Lindzen (1981) and Gill (1982) section 6.14.)

Under more realistic circumstances, for example in non-uniform background flows or for large-amplitude waves, recent studies have shown that the wave evolution can be surprisingly complex. For example, it has been demonstrated that internal waves incident upon a veering wind may be transmitted through a critical level (Shutts 1995, 1998; Broad 1995, 1999). Large-amplitude effects can act to enhance or retard the transmission of wave packets across a reflecting level in a unidirectional shear layer (Sutherland 1999) or into regions where the stratification becomes weaker (Sutherland 1996).

In the absence of shear and in uniformly stratified fluid, plane periodic spanwise uniform internal waves are unstable even at infinitessimally small amplitudes as a result of resonant wave–wave interactions (Mied 1976; Drazin 1977; Lombard and Riley 1996). These results were founded upon earlier work on surface waves by Phillips (1960) and on waves in general (Hasselmann 1967). (Phillips (1981) reviews the development of

* Corresponding address: Department of Mathematical Sciences, University of Alberta, Edmonton, AB T6G 2G1, Canada. e-mail: bruce.sutherland@ualberta.ca

wave interaction theory.) The occurrence of these 'parametric instabilities' has been observed experimentally by Benielli and Sommeria (1996, 1998) and examined numerically by Bouruet-Aubertot *et al.* (1995, 1996) who excited standing internal waves in an oscillating tank with a rectangular horizontal cross-section. At larger amplitudes, but not so large that the waves are overturning, spanwise parametric instabilities may develop, growing at rates comparable with those of the two-dimensional instabilities (Klostermeyer 1991; Lombard and Riley 1996).

The stability of finite-amplitude wave packets in stationary uniformly stratified fluid is governed by different dynamics if the waves are quasi monochromatic (that is, if the wave-packet envelope is of finite vertical and/or horizontal extent). The weakly nonlinear dispersion relation may be used to determine if a finite-amplitude wave-packet envelope grows in amplitude through a process known as modulational instability (Whitham 1965, 1974). Such instability does not necessarily result in wave breaking. If the initial wave amplitude is not too large, the wave packet transfers energy to neighbouring wave numbers through a fundamental nonlinear process known as 'Fermi–Pasta–Ulam' recurrence (Fermi *et al.* 1955). Sutherland (2000) demonstrated that vertically compact, horizontally periodic Boussinesq internal wave packets are unstable to finite-amplitude modulations if the vertical group velocity is a decreasing function of the vertical wave number, *i.e.* the phase lines tilt at angles between 0 and approximately 35 degrees to the vertical. Although the modulational instability is a finite-amplitude effect, the condition for the instability to occur does not depend upon the wave amplitude itself.

A third class of instability, and that which is of primary interest here, arises due to interactions between the waves and the wave-induced mean flow. In their study of large-amplitude internal waves incident upon a critical layer, Fritts and Dunkerton (1984) coined the term 'self acceleration' to describe how the wave-induced mean flow effectively increases the intrinsic phase speed of the waves. Sutherland (2000) proposed that vertically compact, horizontally periodic internal waves become unstable and break if the wave-induced mean flow is greater than the horizontal group velocity of the waves. The amplitude-dependent condition for instability to occur was coined the 'self-acceleration condition'. Such resonant excitation is a special case of the short-wave and long-wave resonant interactions first anticipated by McIntyre (1973) and described analytically by Grimshaw (1977).

Fully nonlinear numerical simulations have demonstrated that the self-acceleration condition does indeed represent well the stability boundary of the waves (Sutherland 2000). The instability occurs because the wave-induced mean flow, which acts most strongly near the centre of the wave packet where the amplitude is largest, locally tilts the isopycnal surfaces until they become convectively overturning. In particular, waves with frequencies very close to, but smaller than, the background buoyancy frequency are unstable to self-acceleration effects at infinitessimally small amplitudes! It has been argued that this explains why turbulence-generated waves in laboratory experiments occur predominantly in a narrow frequency band (corresponding to waves propagating close the maximum vertical group velocity): waves with faster and slower frequencies and with comparable amplitudes are unstable (Sutherland and Linden 1998; Sutherland 2000).

The purpose of the present study is to examine the stability of vertically compact wave packets in a uniform shear flow. In all cases the waves examined propagate upward initially with positive horizontal phase speed, and the shear is prescribed so that the intrinsic (Doppler-shifted) frequency of the waves increases as the wave packet propagates upward. From linear theory, the waves are expected to reflect from a level

where the intrinsic frequency equals the background buoyancy frequency, N. If the waves are of large amplitude, but not so large that the self-acceleration condition is satisfied, the waves are stable initially. As the wave packet propagates toward the reflection level, the intrinsic frequency increases, and the waves may thereby become unstable in one of two ways. First, the intrinsic frequency may become sufficiently large before reflecting that the waves become unstable due to self acceleration. Whether the wave packet becomes unstable depends on whether the wave packet's growth rate is sufficiently large that the instability grows to sufficiently large amplitude before the wave packet encounters the reflecting level. A second mechanism for instability may occur as the wave packet reflects. The superposition of the incident and reflecting wave packets is a disturbance of approximately twice the amplitude of the incident wave packet alone. The amplitude of this disturbance may be so large that the wave packet becomes unstable.

Details of the linear and weakly nonlinear theory for internal waves are given in section 2. The numerical model used to simulate the fully nonlinear evolution of the waves is described in section 3. The results of simulations of horizontally periodic, vertically compact wave packets in uniform shear are described in section 4. The evolution is qualitatively different for horizontally compact wave packets as shown in section 5. Estimates of the critical amplitudes for breaking and transmission across a reflection level are derived in section 6.

2. Theory

This paper is restricted to the study of two-dimensional, Boussinesq internal waves with structure only in the x (horizontal) and z (vertical) directions. In making the Boussinesq approximation, it is assumed that density perturbations due to waves are negligible in the momentum equations except in the buoyancy term.

We further assume that the background density gradient is constant. Thus, the fully nonlinear equations of motion may be written in terms of the vorticity field, ζ, and the vertical displacement field, ξ:

$$\frac{\mathrm{D}\zeta}{\mathrm{D}t} = N^2 \frac{\partial \xi}{\partial x} + \mathcal{D}_\nu \zeta, \tag{1}$$

$$\frac{\mathrm{D}\xi}{\mathrm{D}t} = w + \mathcal{D}_\kappa \xi. \tag{2}$$

Here $\mathrm{D}/\mathrm{D}t$ is the material derivative, w is the vertical velocity, and N is the (constant) background buoyancy frequency. Explicitly, $N^2 \equiv -(g/\rho_0)\, \mathrm{d}\overline{\rho}/\mathrm{d}z$, in which $\overline{\rho}(z)$ is the background density profile, g is the acceleration due to gravity and ρ_0 is a characteristic value of density. In general, $\mathcal{D}_\nu$ and $\mathcal{D}_\kappa$ are operators representing the diffusion of momentum and heat, respectively. In the theory presented below, these are taken to be identically zero, although in practice the numerical model employs an artificial form of the diffusion operators, as discussed in the next section.

Equations (1) and (2) constitute a coupled pair of nonlinear partial differential equations. The velocity field, which appears implicitly in the material derivative, is found from ζ by inverting the Laplacian equation, $\zeta = -\nabla^2 \psi$, to get the stream function ψ, from which the velocity field is immediately determined.

Though explicit analytic solutions of the fully nonlinear equations cannot in general be found, simplifying assumptions can be made to determine the behaviour of periodic waves of small and moderately large amplitude. A review of these results is given below.

(a) *Linear wave theory*

In the absence of background wind, the advection terms in the material derivative of the fully nonlinear equations (1) and (2) are negligible if the waves are of sufficiently small amplitude. Ignoring viscous effects, the resulting coupled pair of linear equations are

$$\frac{\partial}{\partial t}\nabla^2\psi = -N^2\frac{\partial \xi}{\partial x}, \qquad \frac{\partial \xi}{\partial t} = \frac{\partial \psi}{\partial x}. \tag{3}$$

The waves are assumed to be periodic so that one can write $\psi = \Re\{A_\psi \exp(\mathrm{i}\phi)\}$ and $\xi = \Re\{A_\xi \exp(\mathrm{i}\phi)\}$, where $\Re$ denotes the 'real part of', and $\phi = k_x x + k_z z - \omega t$ is the phase of the wave in terms of its wave-number vector (k_x, k_z) and frequency ω, A_ψ is the stream-function amplitude and A_ξ is the amplitude of the vertical-displacement field. Substituting these expressions into Eq. (3) results in an eigenvalue problem which can be solved to give the dispersion relation for small-amplitude internal waves (for example, see Gill 1982):

$$\omega^2 = N^2\frac{k_x^2}{|\mathbf{k}|^2} = N^2\cos^2\Theta. \tag{4}$$

The group velocity of the waves can be determined from this expression and thereby it can be shown that Θ represents the angle of propagation of the waves to the vertical.

The polarization relations and other relevant properties of internal waves are listed in Table 1. For consistency with the results presented here, amplitudes of various fields are given in terms of the amplitude, A_w, of the vertical-velocity field. In particular, Table 1 lists quadratic representations of the wave-induced mean flow, $-\langle\xi\zeta\rangle$, and the vertical flux of horizontal momentum per unit mass, $\langle uw\rangle$, where the angle brackets denote the average over one horizontal wavelength.

(b) *Weakly nonlinear theory*

The dispersion of waves is modified by finite-amplitude effects. These may be represented by a Taylor series expansion of the dispersion relation, which for a one-dimensional system ($\omega = \omega(k)$) is of the form

$$\omega \simeq \omega_0 + (k-k_0)\omega_0' + \tfrac{1}{2}(k-k_0)^2\omega_0'' + |A_0|^2\omega_2, \tag{5}$$

in which A_0 is a measure of the wave amplitude, $\omega_0 = \omega(k_0)$ is the linear-theory prediction for the frequency of the waves of wave number k_0, and the primes denote derivatives with respect to k. The envelope of waves obeying this dispersion relation evolve according to the nonlinear Schrödinger (NLS) equation

$$\mathrm{i}\frac{\partial A}{\partial T} + \frac{1}{2}\omega_0''\frac{\partial^2 A}{\partial X^2} - \omega_2|A|^2A = 0. \tag{6}$$

Here $A(X, T)$ is the (complex) amplitude envelope of the wave packet. It is a function of variables X and T that vary slowly in space and time compared with the wavelength and period of the waves, respectively. The variables are given in a frame of reference moving with the group velocity $c_g = \omega_0'$ (for example, see Whitham 1974, section 17.7).

For moderately large amplitude waves, ω_2 represents the effect of interactions between the waves and the wave-induced mean flow as well as interactions between the waves and the wave-induced first harmonics (waves with wave number $2k_0$).

TABLE 1. PROPERTIES OF SMALL-AMPLITUDE INTERNAL WAVES

Dispersion relation	$\omega = N \cos\Theta$
Phase velocity	$\mathbf{c}_p = (N/k_x)(\cos\Theta, \cos\Theta \cot\Theta)$
Group velocity	$\mathbf{c}_g = (N/k_x)(\cos\Theta \sin^2\Theta, \cos^2\Theta \sin\Theta)$
Horizontal velocity	$A_u = -\tan\Theta A_w$
Vertical displacement	$A_\xi = (\mathrm{i}/N) \sec\Theta A_w$
Vorticity	$A_\zeta = -\mathrm{i}k_x \sec^2\Theta A_w$
Wave-induced mean flow	$-\langle\zeta\xi\rangle = \frac{1}{2}(k_x/N) \sec^2\Theta A_w^2$
Vertical momentum flux	$\langle uw\rangle = -(1/2) \tan\Theta A_w^2$
Stability regimes of finite-amplitude waves	
Vertical modulations	$90° \geq \lvert\Theta\rvert \geq \tan^{-1}(2^{-1/2}) \simeq 35°$
Horizontal modulations	$0 \leq \lvert\Theta\rvert \leq \sin^{-1}(2^{-1/3}) \simeq 53°$
Self acceleration	$\lvert A_w\rvert < \sqrt{2}(N/k_x) \sin\Theta \cos^2\Theta$

Characteristics of small-amplitude internal waves from linear theory, and weakly nonlinear stability characteristics. Values are given in terms of the amplitude of the vertical-velocity field, A_w, the background buoyancy frequency, N, the horizontal wave number, k_x, and the angle of propagation of the waves to the vertical, Θ.

The calculation of ω_2 can be quite involved. For the case of internal waves, only the results of two special cases will be considered here: the vertical dispersion of horizontally periodic waves, and the horizontal dispersion of internal wave modes bounded above and below. In both cases the background stratification and wind speed are assumed to be constant.

In considering the weakly nonlinear dispersion of vertically compact, horizontally periodic waves, the horizontal wave number, k_x, is assumed to remain constant for all time, but the vertical wave number, k_z, may vary. With some exceptions, the time evolution of the wave packet is given approximately by Eq. (6) with $\omega_0'' \equiv \partial^2\omega/\partial k_z^2$ and

$$\omega_2 = 2\omega_0 \frac{|\mathbf{k}|^4}{N^2 k_x^2} = 2\omega_0 \sec^4\Theta \frac{k_x^2}{N^2}, \tag{7}$$

where $\omega_0 \equiv \omega$ in Eq. (4), and A_0 in Eq. (5) is taken to be the amplitude of the vertical-velocity field, A_w. This result is valid provided the waves do not propagate upward at the fastest group velocity, in which case $\omega_0'' = 0$ and a higher-order partial differential equation than Eq. (6) is required. For Eqs. (6) and (7) to be valid it is also necessary for the amplitude of the waves to be sufficiently small; the equations break down if the waves are of sufficiently large amplitude that they resonantly excite the mean flow (Mcintyre 1973; Grimshaw 1977). Sutherland (2000) showed that the wave packets become unstable to convective overturning as a result of this resonant interaction. The critical amplitude at which this occurs is given by the self-acceleration condition, Eq. (10).

The weakly nonlinear dispersion of vertically bounded wave packets has been considered by Grimshaw (1977). The vertical structure of the waves is represented by a

series of discrete modes and the wave packet is free to disperse horizontally. The wave-packet evolution is given by Eq. (6) with $\omega_0'' \equiv \partial^2\omega/\partial k_x^2$ and

$$\omega_2 = -12\frac{k_x}{c_{px}}\frac{\sigma^3}{1-4\sigma^3} \simeq -12\omega_0 \sec\Theta\frac{\sin^6\Theta}{1-4\sin^6\Theta}\frac{k_x^2}{N^2}, \tag{8}$$

where $\sigma = c_{gx}/c_{px} \simeq \sin^2\Theta$ (for high-order vertically confined modes), and $A_0 \equiv A_w$, as above. c_{px} is the horizontal phase speed and c_{gx} is the horizontal group velocity.

The modulational stability of a finite-amplitude wave packet may be assessed using Whitham's theory (Whitham 1965). Briefly, this predicts that the finite-amplitude form of the group velocity of waves obeying the dispersion relation Eq. (5) is

$$c_{g\pm} \doteq \omega_0' \pm A(\omega_2\omega_0'')^{1/2}. \tag{9}$$

If the radical has a real value, the wave packet is stable and divides into two disturbances propagating at different group velocities. If the radical is imaginary, the wave packet is unstable and grows in amplitude as it evolves.

Applying the stability criterion to the case of vertically compact and horizontally periodic internal waves, it is found that the waves are stable if $\omega_0'' > 0$. That is, the wave-packet envelope does not increase in amplitude if the phase lines tilt at angles $35° < |\Theta| \leq 90°$. The wave packet is unstable otherwise. Modulational stability and instability are demonstrated in the numerical simulations presented in section 4. Although modulational instability implies that the wave packet grows in amplitude, it is not necessarily true that the waves ultimately break as a result. Provided the initial amplitude of the waves is not too large, the wave packet first grows in amplitude then subdivides into a sequence of smaller wave packets, as was described by Benjamin and Feir (1967) in their study of deep-water waves.

When the stability criterion is applied to the case of modes spanning a vertically bounded domain, it is found that the wave packets are unstable if $\Theta > 53°$ (Grimshaw 1977; Sutherland 2000).

(c) *Self acceleration of internal waves*

For sufficiently large-amplitude waves, the wave-induced mean flow is excited resonantly by wave–wave interactions (Mcintyre 1973; Grimshaw 1977). Resonant excitation occurs when the wave-induced mean flow speed equals the horizontal group velocity of the waves. Using linear theory estimates Sutherland (2000) argued that this occurs when the amplitude of the vertical displacement field, $A_\xi = \lambda_x \sin 2\Theta/(8\pi^2)^{(1/2)}$, where λ_x is the horizontal wavelength and Θ gives the angle of the tilt of the phase lines to the vertical (or, equivalently, the angle of the wave-number vector to the horizontal). From the dispersion relation, $\Theta = \cos^{-1}(\omega/N)$. In terms of the amplitude of the vertical-velocity field, A_w, the critical value is given by

$$A_w^{\text{crit}} = (2^{1/2}\sin\Theta\cos^2\Theta)\frac{N}{k_x}. \tag{10}$$

The self-acceleration condition asserts that waves are unstable and ultimately break if the amplitude of the vertical-velocity field exceeds that given by Eq. (10), i.e. if $A_w > A_w^{\text{crit}}$. It follows from Eq. (10) that, if Θ is close to zero or 90°, the waves are unstable at very small amplitudes.

For a wave packet incident upon a reflecting level, the superposition of the incident and reflecting wave packet is a disturbance of approximately twice the amplitude.

Although the incident wave packet may be stable to self-acceleration effects, the superimposed incident and reflected waves are unstable if the amplitude of the incident wave exceeds $A_w^{\text{crit}}/2$. That is, if

$$A_w > A_w^{\text{break}} = (2^{-1/2} \sin\Theta \cos^2\Theta)\frac{N}{k_x}. \tag{11}$$

Table 1 summarizes the finite-amplitude stability regimes described in sections 2(b) and (c).

(*d*) *Internal wave reflection and caustics*

The intrinsic frequency of internal waves is Doppler shifted as they propagate vertically in wind shear. If the background velocity profile, $\overline{U}(z)$, varies slowly with height compared with the vertical wavelength of the waves, the intrinsic frequency is $\Omega = \omega_0 - k_x\overline{U}$, in which $\omega_0 = k_x c_{px}$ is constant.

Suppose a wave packet propagates upwards with positive horizontal phase speed, c_{px}, with respect to the background wind at some level. If the background wind speed increases linearly with height, then eventually the wave packet will encounter a critical level, being the height at which the background wind equals the horizontal phase speed ($\Omega = 0$). Ray theory predicts that the (two-dimensional) wave asymptotically approaches such a critical level and must ultimately overturn and break (Bretherton 1966; Lighthill 1978).

The converse situation is relevant here. If the background wind decreases linearly with height then the intrinsic frequency of the waves equals the background buoyancy frequency at some height ($\Omega = N$). Above this level small-amplitude waves are evanescent: the waves do not propagate and their amplitude decreases exponentially. Ray theory predicts that incident waves reflect downward at this height, which is referred to hereafter as a 'reflecting level'. This boundary between the region of incident and reflected waves and the region of evanescent, exponentially decaying waves is also referred to as a 'caustic'.

When internal waves of moderately large amplitude are incident upon a reflecting level, the superposition of the upward-propagating incident and downward-propagating reflected wave is a disturbance of approximately twice the amplitude of each wave taken individually. The wave-induced mean flow, which to first order is proportional to the amplitude squared, increases by approximately quadruple its value near the reflecting level. Numerical simulations have shown that interactions between the waves and the wave-induced mean flow increase the intrinsic frequency of the waves as their amplitude increases (Sutherland 1996a). Thus, weakly nonlinear effects can act to enhance the reflection of waves (with positive phase speed) in a background localized shear flow whose speed decreases with height to a smaller value, but not so small that a reflecting level is present. In this case, the wave-induced mean flow may increase the intrinsic frequency of the waves to such a large value that the waves are evanescent above the shear layer. Likewise it has been shown that the intrinsic frequency of a moderately large-amplitude wave packet decreases as its amplitude decreases, and thereby enhanced transmission of a wave packet across a reflecting level may occur.

Sutherland (1996, 1999) examined the reflection of internal waves in hyperbolic tangent shear flows, in which case it was a simple matter to diagnose the characteristics of the reflected and transmitted waves well above and below the shear layer. In the present study, the background is taken to be a constant-shear flow. Thus, although the transmission of large-amplitude waves across a reflecting level is anticipated, it

is expected that the waves must ultimately encounter a level where the entire wave packet reflects. Nonetheless, numerical simulations demonstrate remarkably different behaviours for horizontally periodic and compact wave packets.

3. Description of the numerical model

The propagation of internal waves is examined using a fully nonlinear numerical model that solves Eqs. (1) and (2). The domain is taken to be a periodic channel flow with free-slip upper- and lower-boundary conditions. The vertical boundaries are taken to be so far from the waves, that they can effectively be ignored. In simulations of horizontally compact waves, the horizontal extent of the domain is set to be over ten times larger than the wave-packet extent. Domain-size doubling tests confirm that the horizontal extent of the domain is sufficiently large that the horizontal periodicity of the domain does not affect the wave-packet evolution. In simulations without wave breaking, typically the resolution is sufficiently fine that at least 40 grid points span one vertical wavelength of the wave packet under consideration. In simulations with wave breaking, the vertical resolution is four times greater. A recent detailed description of the model is given by Sutherland (1999).

Of interest here are the dynamics of nonhydrostatic waves, which have non-negligible vertical velocity compared with the horizontal velocity and whose intrinsic frequency is comparable with the background buoyancy frequency, N. Coriolis forces are neglected.

The effects of viscosity are assumed to be negligible. Nonetheless, it is necessary to include the dissipation-like terms $\mathcal{D}_\nu$ and $\mathcal{D}_\kappa$ in order to eliminate the growth of small-scale numerical noise. Explicitly, $\mathcal{D}_\nu$ is the product of an effective Reynolds number, Re, times a Laplacian diffusion operator acting only on horizontal scales smaller than the horizontal wavelength of the initial wave packet. Here the value $\mathrm{Re} = 10\,000$ is used, based on the horizontal wave number, k_x, of the initial waves and the background buoyancy frequency, N. This value of the Reynolds number is chosen so that the viscous dissipation time-scale is longer than the duration of any simulation, typically 64 buoyancy periods. One buoyancy period is $T = 2\pi/N$. Explicitly, the dissipation time-scale is

$$T_{\mathrm{diss}} \sim (\nu|\mathbf{k}|^2)^{-1} = \mathrm{Re}(\mathcal{L}^2|\mathbf{k}|^2/\mathcal{T})^{-1} = \mathrm{Re}\cos^2\Theta/(2\pi N)$$

where $\mathcal{L}$ and $\mathcal{T}$ represent characteristic length- and time-scales, respectively, of the waves.

The simulations are initialized with a wave packet defined in terms of the vertical-velocity field by

$$w(x, z) = \Re[W(x, z)\exp\{\mathrm{i}(k_x x + k_z z)\}] \tag{12}$$

in which $W(x, z)$ prescribes the structure of the wave-packet envelope. The horizontal wave number, k_x, is set to be positive and the vertical wave number, k_z, is set to be negative, so that in time the wave packet propagates upward and to the right.

The wave packet is prescribed so that initially the amplitude envelope decreases exponentially about the wave-packet centre. The waves may be either horizontally periodic with

$$W_{\mathrm{PW}}(x, z) = A_w \exp(-|z|/\sigma_z), \tag{13}$$

or horizontally compact, the envelope being Gaussian in the horizontal:

$$W(x, z) = A_w \exp(-|z|/\sigma_z)\exp(-x^2/2\sigma_x^2). \tag{14}$$

TABLE 2. PREDICTED PROPERTIES OF INTERNAL WAVES

$-k_z/k_x$	$A_w k_x/N$	Θ	ω/N	$(c_{gx}, c_{gz})k_x/N$	$\{-\langle\zeta\xi\rangle\}_{\max}k_x/N$	$\{\langle uw\rangle\}_{\max}(k_x/N)^2$
0.4	0.02	21.8°	0.93	(0.13, 0.32)	2.5×10^{-4}	8.0×10^{-5}
0.4	0.30	21.8°	0.93	(0.13, 0.32)	5.6×10^{-2}	1.8×10^{-2}
0.7	0.02	35.0°	0.82	(0.27, 0.39)	3.6×10^{-4}	1.4×10^{-4}
0.7	0.30	35.0°	0.82	(0.27, 0.39)	8.2×10^{-2}	3.2×10^{-2}
1.4	0.02	54.5°	0.58	(0.39, 0.27)	1.0×10^{-3}	2.8×10^{-4}
1.4	0.30	54.5°	0.58	(0.39, 0.27)	2.3×10^{-1}	6.3×10^{-2}

$-k_z/k_x$	$-s/N$	$A_w^{\text{break}}k_x/N$	$A_w^{\text{transmit}}k_x/N$
0.4	0.002	0.23	0.18
0.7	0.004	0.27	0.21
1.4	0.016	0.19	0.25

Predicted properties of internal waves analysed in detail here, including maximum values of the non-dimensional wave-induced mean flow ($\langle\zeta\xi\rangle$) and the vertical momentum flux per unit mass ($\langle uw\rangle$) for the wave packets. The second table gives predicted critical amplitudes for breaking (see Eq. (11)) and transmitted (see Eq. (16)) internal waves in uniform shear. k_z is the vertical wave number, k_x is the horizontal wave number, A_w is the amplitude of the vertical-velocity field, N is the background buoyancy frequency, Θ is the angle of propagation of the waves to the vertical, c_{gx} is the horizontal group velocity, c_{gz} is the vertical group velocity, and s is the shear strength.

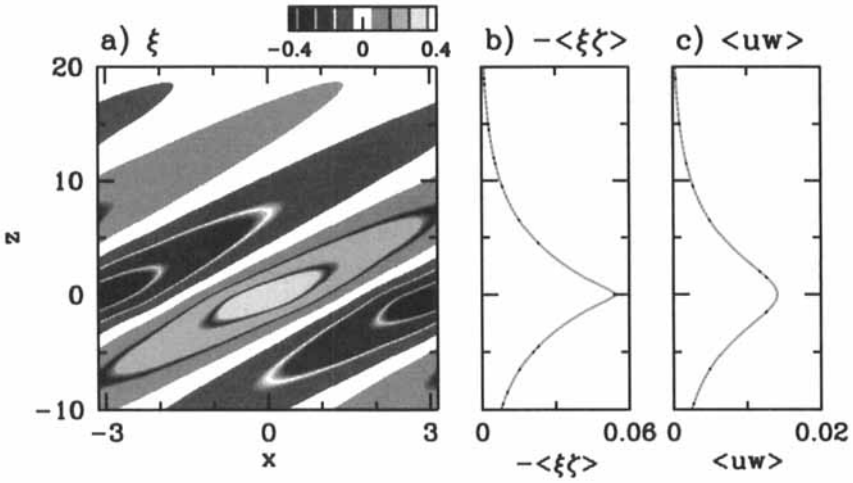

Figure 1. Initial state of horizontally periodic internal waves showing (a) the vertical-displacement field (ζ), (b) the wave-induced mean flow ($\langle\zeta\xi\rangle$) and (c) the vertical flux of horizontal momentum per unit mass ($\langle uw\rangle$), associated with this wave packet. Here $k_x = 1$ and $N = 1$ in arbitrary units. See text for further details.

A_w is the amplitude of the vertical-velocity field and σ_x and σ_z are the horizontal and vertical extents of the wave packet, respectively. In all studies discussed here the vertical extent is given in terms of the horizontal wave number by $\sigma_z = 10/k_x$ and the extent of horizontally compact wave packets is given by $\sigma_x = 10/k_x$.

The background flow is given by $\overline{U} = U_0 + sz$, where s is a small negative constant. In studies of horizontally periodic waves it is convenient to set $U_0 = -c_{px}$ so that the horizontal phase speed of the waves is effectively zero in the small-amplitude limit. In studies of horizontally compact waves $U_0 = 0$. Superimposed on the mean flow is the calculated wave-induced mean flow, $-\langle\zeta\xi\rangle$. Initially this results in a small increase in $\overline{U}$ over a range σ_z about $z = 0$. Simulations show that as the wave packets propagate

upward in time, away from the origin, the residual mean flow is just $U_0 + sz$. If the wave-induced mean flow is not introduced initially, the residual mean flow near the origin is found to be approximately $U_0 + sz + \langle \zeta \xi \rangle$, after the wave packet has propagated away.

Simulations are performed in which the evolution of horizontally periodic and horizontally compact wave packets is examined as a function of amplitude, A_w, phase tilt, $\Theta = |\tan^{-1}(k_z/k_x)|$, and shear strength, s. In practice, the length and time-scales in the simulations are established by setting $k_x \equiv 1$ and $N_0 \equiv 1$, respectively. For ease of interpretation and extension of these results to atmospheric and oceanic flows, results are given in dimensionless units where practical. Thus, the shear strength is given as a fraction of the buoyancy frequency, and the amplitude, A_w, is given as a fraction of N/k_x. Conversion to other physical quantities may be calculated using Table 1.

Although a wide range of simulations were performed, only a subset of these are reported upon in detail here. The vertical wave number is set so that $k_z/k_x = -0.4$, -0.7 and -1.4. These correspond to wave packets that are unstable, marginally stable, and stable to finite-amplitude modulations, respectively. The second case corresponds to wave packets moving upward at approximately the fastest vertical group velocity with respect to k_z. The last case corresponds to wave packets moving from left to right with approximately the fastest horizontal group velocity. In most simulations reported here the shear strength is set so that $s/N = -0.002$, -0.004 and -0.016 for $k_z/k_x = -0.4$, -0.7 and -1.4, respectively. The values are chosen so that the reflection level is situated a distance between 15 and $20 c_{gz} T$ above the initial position of the wave packet. Thus, in theory the wave packet propagates to the height of the reflection level after 15 to 20 buoyancy periods. The predicted properties of the internal waves are listed in Table 2.

The initial state of a simulation of a horizontally periodic wave packet is shown in Fig. 1. This shows the normalized vertical-displacement field, $\xi(x, z)$, the corresponding wave-induced mean flow profile, $-\langle \xi \zeta \rangle$, and the vertical flux of horizontal momentum per unit mass, $\langle uw \rangle$. Note that the momentum flux is positive, corresponding to the upward transport of forward momentum.

4. HORIZONTALLY PERIODIC WAVES

The evolution of a vertically compact wave packet is examined as a function of A_w, Θ, and the background shear strength, s. In this section, the waves are taken to be initially horizontally periodic with structure given by Eqs. (12) and (13) with $\sigma_z = 10/k_x$.

In the absence of shear, large-amplitude wave packets evolve quite differently depending on their vertical wave number. This is illustrated in Fig. 2, which shows the evolution of small- and large-amplitude wave packets with wave numbers $k_z/k_x = -0.4$ (Figs. 2(a) and (d)), -0.7 (Figs. 2(b) and (e)), and -1.4 (Figs. 2(c) and (f)). The plots show vertical time series over approximately 64 buoyancy periods of second-order accurate estimates of the wave-induced mean flow, $-\langle \zeta \xi \rangle$. The vertical axis is normalized by the product of T with the vertical group velocity, c_{gz}, predicted by linear theory. The time series itself is normalized by the maximum value of $-\langle \zeta \xi \rangle$ calculated from linear theory at time $t = 0$ (see Tables 1 and 2).

In the small-amplitude cases, (Figs. 2(a), (b) and (c)), the wave packet moves upward at a steady speed equal to the vertical group velocity, c_{gz}, as expected from linear theory. The least dispersion occurs for the wave packet with vertical wave number $k_z = -0.7 k_x$. Such behaviour is anticipated because, from the linear dispersion relation for internal

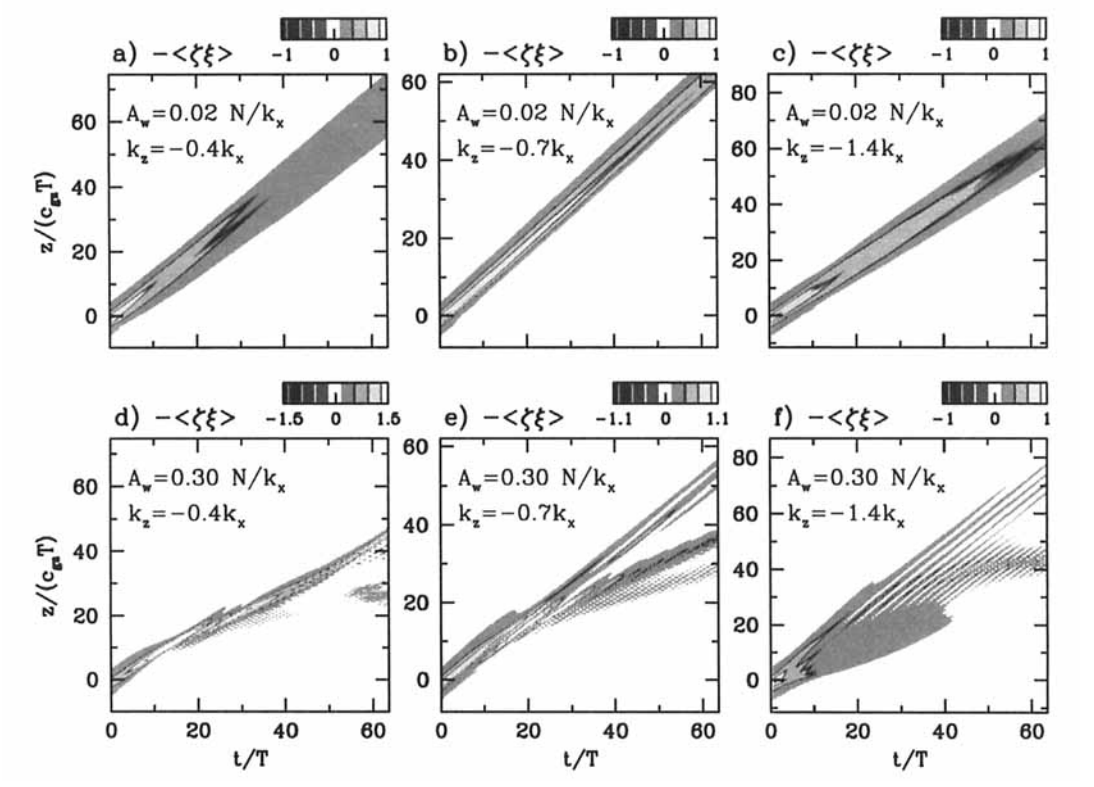

Figure 2. Time series of the normalized wave-induced mean flow in six simulations of small- and large-amplitude wave packets in flow with no shear (see text). The amplitude, A_w, and vertical wave number, k_z, corresponding to each simulation are shown. N is the background buoyancy frequency and k_x the horizontal wave number. See text for further details.

waves, $\partial^2\omega/\partial k_z^2 = 0$ if $k_z/k_x = -2^{-1/2} \simeq -0.707$, which corresponds to internal waves propagating vertically with the fastest group velocity.

The wave-packet dispersion is quite different for the corresponding large-amplitude internal waves for which the vertical-velocity field is $A_w = 0.3N/k_x$. In Fig. 2(d) the wave packet increases in amplitude initially reaching maximum amplitude after approximately 14 buoyancy periods. This behaviour agrees with the predictions of Whitham's stability theory applied to horizontally periodic internal waves, which claims that weakly nonlinear modulated wave packets are unstable if $|k_z/k_x| < 2^{-1/2} \simeq 0.7$ (Sutherland 2000). The ensuing evolution is described by Benjamin and Feir (1967) and may be determined by inverse-scattering theory. Overall, weakly nonlinear effects act to limit the lateral dispersion of the wave packet while reducing its vertical group velocity.

Figure 2(f) shows the evolution of a stable large-amplitude wave packet with $k_z = -1.4k_x$. Here, the amplitude of the wave packet is largest at $t = 0$ and the wave packet rapidly subdivides into a train of solitary waves following the well recognized Fermi–Ulam–Pasta recurrence.

The transitional case with $k_z = -0.7k_x$ is shown in Fig. 2(e), which shows that the wave packet peaks in amplitude near time $t = 20T$, and thereafter subdivides into three distinct groups of wave packets.

Because of the complex dispersion characteristics of large-amplitude internal waves, the analysis of their evolution in a shear flow is subdivided into three cases representative

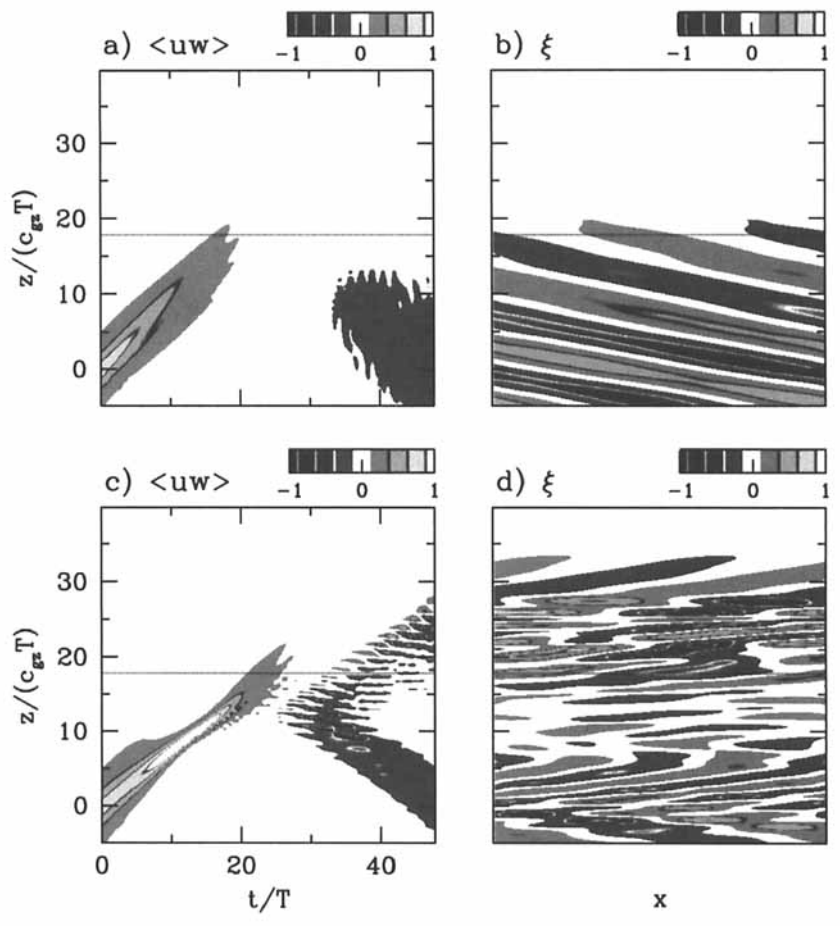

Figure 3. (a) Time series of the normalized vertical flux of horizontal momentum per unit mass for a wave packet with vertical wave number $k_z = -0.4k_x$ and amplitude $A_w = 0.02N/k_x$; (b) the normalized vertical-displacement field shown for this simulation at time $t \simeq 48T$; (c) and (d) show plots corresponding to (a) and (b), respectively, but for a simulation of a large-amplitude wave packet with $A_w = 0.30N/k_x$. In both simulations the background shear is $s = -0.002N$. See text for further details.

of modulated wave packets that are unstable, marginally stable, and stable. These are examined sequentially in each subsection below.

(*a*) *Case:* $k_z = -0.4k_x$

In this case, finite-amplitude wave packets are unstable to modulational instability. The evolution of small- and large-amplitude wave packets in the presence of constant background shear with $s = -0.002N$ is illustrated in Fig. 3. The plot in Fig. 3(a) shows the vertical time series of $\langle uw \rangle$, the vertical flux of horizontal momentum per unit mass, as the wave packet evolves over 64 buoyancy periods, $T = 2\pi/N$. The wave packet is of relatively small amplitude, $A_w = 0.02N/k_x$. The field is normalized by the maximum initial value of $\langle uw \rangle$ (see Table 1). A horizontal dashed line is drawn to indicate the height of the reflection level (the height where the Doppler-shifted frequency of the wave equals the buoyancy frequency N). At early times $\langle uw \rangle$ is positive, corresponding to the upward propagation of forward momentum. As the small-amplitude wave packet approaches the reflection level, however, the vertical momentum flux decreases and

is redirected downward between times $t = 20T$ and $30T$. Figure 3(b) illustrates the structure of the reflected waves at time $t \simeq 48T$. The plot shows contours of the vertical displacement field, ξ, normalized by the maximum value of this field at time $t = 0$ (see Table 1). The horizontal scale spans one wavelength and the vertical scale is the same as that in Fig. 3(a). The downward left-to-right tilt in the phase lines of the waves is consistent with downward-propagating, reflected waves.

In comparison, Figs. 3(c) and (d) show time series of $\langle uw \rangle$ and a snapshot of the vertical-displacement field at time $t \simeq 48T$, but shown here for large-amplitude waves with $A_w = 0.30N/k_x$. As in Fig. 2(b), the maximum momentum flux increases over time initially and the group velocity is smaller. However, a significant fraction of the momentum flux is reflected downward before the wave packet reaches the height of the reflection level. Indeed, the redistribution of momentum by the wave packet is quite complicated. The vertical displacement field in Fig. 3(d) shows that the reflected wave packet near $z = 0$ is composed of waves with half the horizontal wavelength of the initial wave packet. A significant proportion of the wave packet has penetrated well above the reflection level and continues to propagate upward above $z \simeq 30c_{gz}T$, as indicated by the upward left-to-right tilt of phase lines. It is interesting to note that the momentum flux associated with the upward propagating waves is predominantly negative above the reflection level. The detailed mechanism for the generation of super-harmonic waves (of smaller horizontal wavelength) and the implication of these structures for momentum transport and deposition merits further investigation but is beyond the scope of this work. Certainly, the phenomena are 'real' in the sense that their qualitative features are unaltered in resolution-doubling tests.

If $|k_z| < k_x/2^{1/2}$, and in particular if $k_z = -0.4k_x$, the amplitude of the weakly nonlinear wave packet increases even in the absence of background shear due to modulational instabilities. This explains why the large-amplitude wave packet reflects well below the reflecting level in the constant-shear case examined here. As the wave packet grows in amplitude, its intrinsic frequency increases, so the effective reflecting level occurs at a lower height.

The transmission of a wave packet incident upon a reflecting level may also be enhanced due to weakly nonlinear effects. This occurs because the intrinsic frequency of the wave decreases when its amplitude decreases. As the trailing edge of the incident wave packet approaches the reflecting level, the amplitude of the incident and reflected waves decreases, and the resulting decrease in the intrinsic frequency of the waves enables a proportion of the incident wave to penetrate above the reflecting level.

Indeed, in the constant-shear case examined here, a proportion of the large-amplitude wave packet is found to transmit above this level. However, as the transmitted proportion of the wave packet continues to propagate upward, it continues to be Doppler shifted by the decreasing background wind, and it is expected that it will eventually reflect or dissipate.

The dynamics of the reflecting and transmitting wave packets are further complicated by interactions between the reflected and transmitted waves. For sufficiently large-amplitude waves, these result in the permanent deposition of momentum to the mean flow.

To illustrate this, Fig. 4 shows vertical time series of ΔU and $-\langle \zeta \xi \rangle$. The former is the calculated difference between the horizontally averaged flow at each time and the initial background shear, $U(z) = U_0 + sz$. Figures 4(a) and (b) show these time series for a simulation of small-amplitude waves with $k_z = -0.4k_x$ and $A_w = 0.02N/k_x$. As the wave packet propagates upward in a shear flow with $s = -0.002N$ and reflects from a reflecting level, the two profiles are approximately the same at corresponding times.

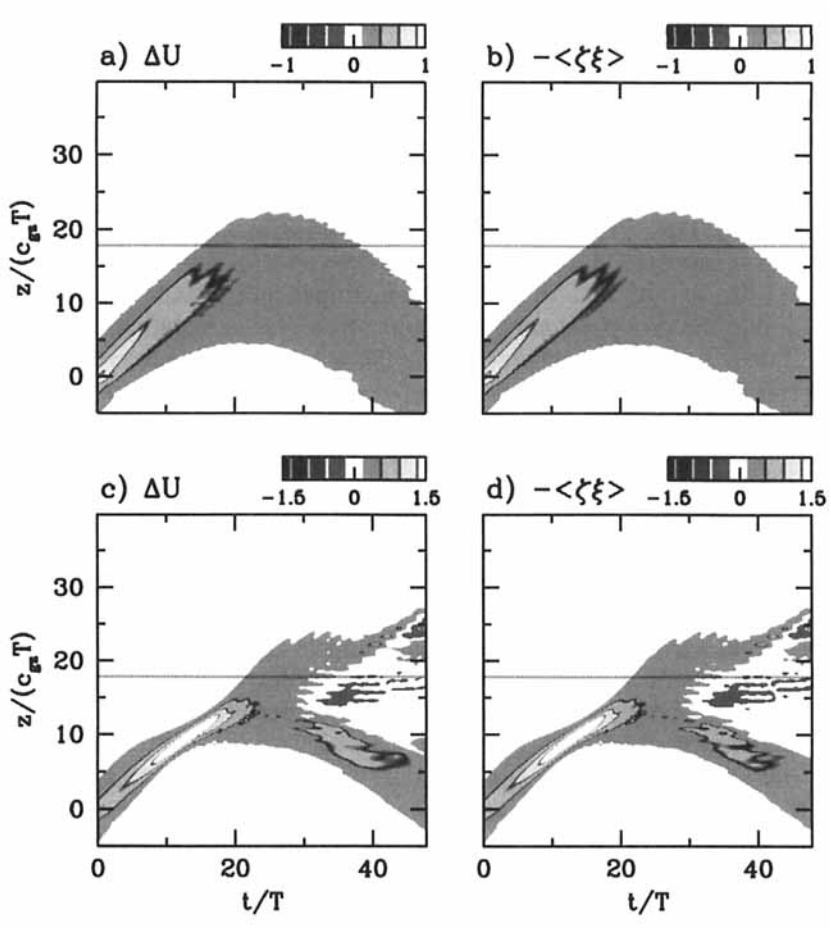

Figure 4. Time series of (a) ΔU and (b) $-\langle \xi \zeta \rangle$ for a simulation with $k_z = -0.4k_x$ and $A_w = 0.02N/k_x$. (c) and (d) show plots corresponding to (a) and (b), respectively, but for a simulation of a large-amplitude wave packet with $A_w = 0.30N/k_x$. In both simulations the background shear is $s = -0.002N$. The horizontal line superimposed on each plot indicates the location of the reflection level predicted by linear theory. See text for further details.

Figures 4(c) and (d) show the same fields but for a simulation of large-amplitude waves with $A_w = 0.3N/k_x$. Although near time $t = 0$ the two fields are the same, they differ significantly when the waves partially reflect. The difference indicates that momentum has been deposited permanently to the mean flow.

This conclusion is supported by the observed behaviour of the vertical-displacement field as it evolves over time in a digitized movie. The field is analysed in a frame of reference moving with the (positive) horizontal phase speed, c_{px}, of the waves. As the waves move upward initially, the amplitude of the waves changes but their phase remains stationary at any fixed point in space. However, as they reflect, interactions between the incident and reflected waves excite waves of smaller horizontal wavelength (for example, see Fig. 3(d)). These smaller-scale disturbances have lower horizontal phase speeds than the incident waves; they move backward in the frame of reference moving at speed c_{px}. In time, viscosity efficiently dissipates these small-scale waves and their associated momentum is deposited to the mean flow.

In general, there are three possible mechanisms for momentum deposition due to reflection, each of which occurs because the result of the superposition of the incident and reflected waves is a disturbance of larger amplitude.

The first possibility, which is apparent here, is that interactions between the large-amplitude incident and reflected waves, excite waves of shorter horizontal wavelengths. Ultimately, the energy associated with these smaller-scale disturbances is dissipated more efficiently by viscosity.

A second, more efficient, possibility occurs if the incident wave is of sufficiently large amplitude that, although the wave alone is not overturning, its superposition with the reflected wave is an overturning disturbance. That is, there may be regions in the fluid where the sum of the background and fluctuation density increases with height. If the wave-field evolves sufficiently slowly, convective instabilities will have time to grow.

A third, but related, mechanism for momentum deposition is through interactions between the superimposed disturbances and the wave-induced mean flow which drive the flow to convective instability. The amplitude of the incident waves may initially be much smaller than that required for overturning, for this instability due to 'self acceleration' to take place. However, the superposition of the incident and reflecting waves approximately doubles the amplitude of the superimposed disturbance and quadruples the associated wave-induced mean flow. Thus, incident waves that are stable to self-acceleration effects may be unstable upon reflection.

Figure 5 assesses the stability of the reflecting large-amplitude waves to super-harmonic excitation and to convective instability. Figure 5(a) shows that super-harmonic disturbances (of horizontal wave number $2k_x$) are strongly excited at times $t > 25T$. Energy-transfer diagnostics (not shown) confirm that energy is tranferred directly from wave number k_x to $2k_x$; energy is not significantly transferred to or from the mean flow. The convective stability of the flow is assessed by computing the minimum value of $\Delta N^2 \equiv -(g/\rho_0)\, \mathrm{d}\rho/\mathrm{d}z$, the change in the buoyancy frequency due to the perturbation density field, $\rho(x, z, t)$. If $\Delta N^2 < -N^2$, the disturbances are overturning somewhere in the flow field. Figure 5(b) shows that the flow field is convectively stable over the times shown. The sub-harmonic waves are thus generated solely as a consequence of the nonlinear interaction between the incident and reflecting waves.

(*b*) *Case:* $k_z = -0.7k_x$

In this case the magnitude of the vertical wave number, $|k_z| \simeq k_x/2^{1/2}$, which corresponds to a wave packet propagating with the fastest vertical group velocity, and horizontally periodic wave packets are marginally stable to growth due to modulations.

As in Fig. 3, Fig. 6 shows the evolution and structure of small- and large-amplitude waves reflecting in a constant shear flow with $s = -0.004N$. The strength of the shear is chosen so that the normalized height of the reflecting level, $z_c/(c_{gz}T)$, is comparable to that for the case with $k_z = -0.4k_x$.

The time evolution of the normalized momentum flux is shown in Fig. 6(a) for small-amplitude waves with $A_w = 0.02N/k_x$. This clearly shows the wave packet transporting forward momentum upwards until it reaches the reflecting level at time $t \simeq 20T$ (about 20 buoyancy periods). After this time, the wave packet reflects and transports momentum downwards. The vertical-displacement field at time $t \simeq 48T$, shown in Fig. 6(b), illustrates the downward tilt of phase lines characteristic of downward momentum transport by rightward propagating waves.

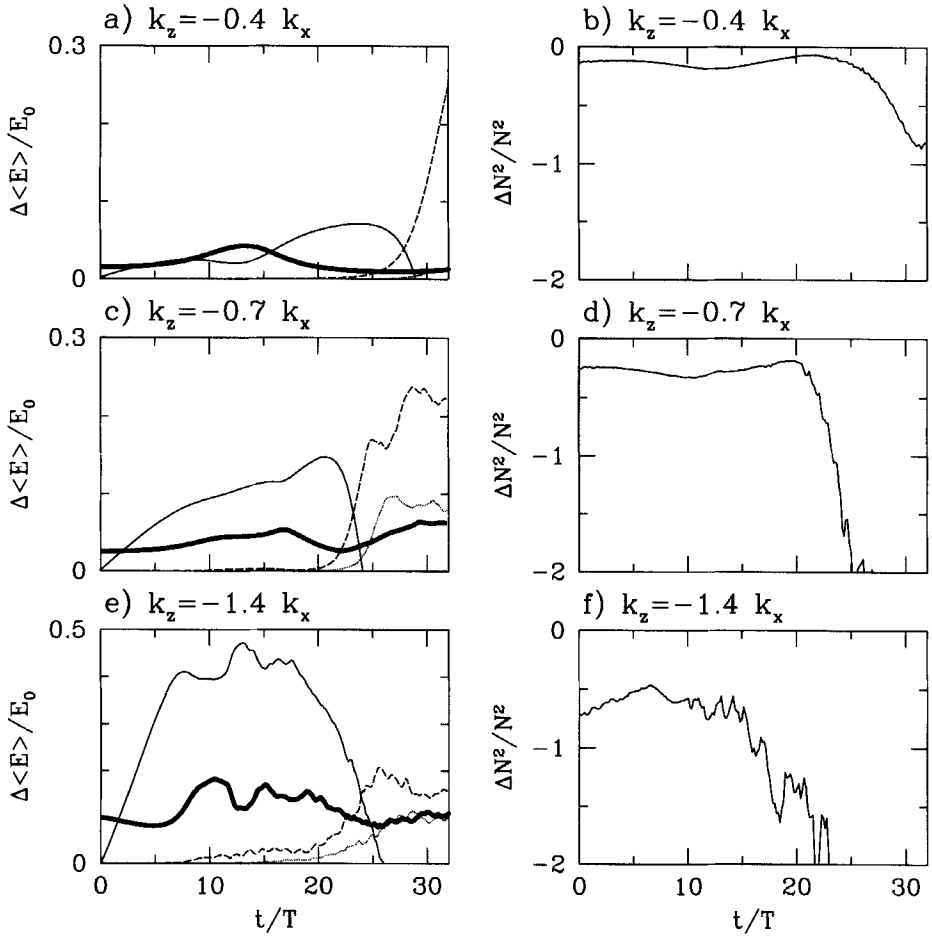

Figure 5. Superharmonic excitation and convective instability cases with $k_z = -0.4k_x$, $s = -0.002N$ ((a) and (b)), $k_z = -0.7k_x$, $s = -0.004N$ ((c) and (d)), and $k_z = -1.4k_x$, $s = -0.016N$ ((e) and (f)). $A_w = 0.15N/k_x$ in each case. All plots show evolution over time from $t = 0$ to $32T$. Plots (a), (c) and (e) show the change in energy from initial values in different harmonics: energy associated with disturbances of horizontal wavenumber k_x (thin solid line), $2k_x$ (long-dashed line), $3k_x$ (dotted line); and energy difference between mean flow and initial background shear (thick solid line). All values are normalized by the initial energy associated with the waves. Plots (b), (d) and (f) show the minimum value of $\Delta N^2/N^2$. Disturbances are overturning if this value is less than -1. See text for further details.

The evolution of large-amplitude waves with $A_w = 0.30N/k_x$ is shown in Fig. 6(c). As in the case with $k_z = -0.4k_x$, the waves reflect from a level well below that predicted by linear theory. Unlike that case, however, the reflecting wave packet remains more coherent: at time $t \simeq 24T$ the momentum flux exhibits a large negative peak near $z = 6c_{gz}T$, and the momentum flux is negligible above $z \simeq 10c_{gz}T$. Shortly after $t \simeq 24T$ the waves overturn and the simulation is terminated as small-scale structures in the convectively unstable region grow in amplitude at time and length scales too small to be resolved. The details of this convective instability and the resulting deposition of momentum certainly merits more research but would be a moot exercise here, the simulation being restricted to two-dimensional motions.

It is nonetheless worth emphasizing this important result: wave breaking may occur at a reflecting level! That wave breaking may occur near a critical level, where the

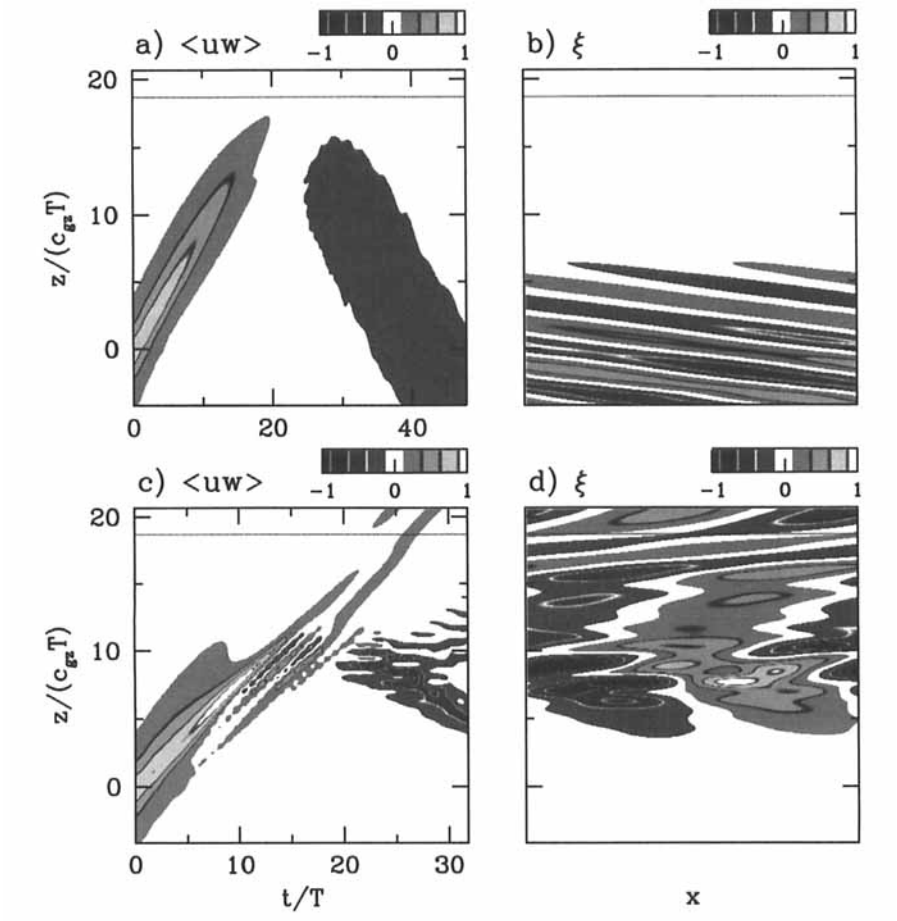

Figure 6. As in Fig. 3 but for a wave packet with $k_z = -0.7k_x$ and $A_w = 0.02N/k_x$ ((a) and (b)) and $A_w = 0.30N/k_x$ ((c) and (d)). The background shear is $s = -0.004N$. Note that the time series in (c) is shown over a shorter time than in (a). The vertical-displacement field in (b) is shown at time $t \simeq 48T$ and that in (d) is shown at time $t \simeq 24T$. See text for further details.

horizontal phase speed of the waves equals the background flow speed, is well known (Booker and Bretherton 1967; Bretherton 1969). At a reflecting level, however, it is often assumed that the flux of momentum is redirected, but not deposited, to the mean flow. This simulation, and other simulations of large-amplitude waves not reported here, demonstrate that momentum can be deposited to the mean flow if the incident waves are of sufficiently large amplitude.

In the simulation of large-amplitude waves, with $k_z = -0.7k_x$, self acceleration may ultimately be the source of instability and the cause for momentum deposition to the mean flow by way of wave breaking. This may be inferred from Fig. 6(d), which shows the vertical-displacement field at time $t \simeq 24T$. Though a small proportion of the wave packet extends above the reflecting level at this time, most of it is centred near $z = 7c_{gz}T$. Here the tilt of the phase lines is almost vertical and the amplitude of the disturbance is larger than the initial wave amplitude. These features in combination lead one to anticipate that the disturbance may become unstable due to self acceleration.

Further evidence of the significant effects of self acceleration is illustrated in Fig. 7. As in Fig. 4, this shows time series of the normalized ΔU and $-\langle \zeta \xi \rangle$ profiles for

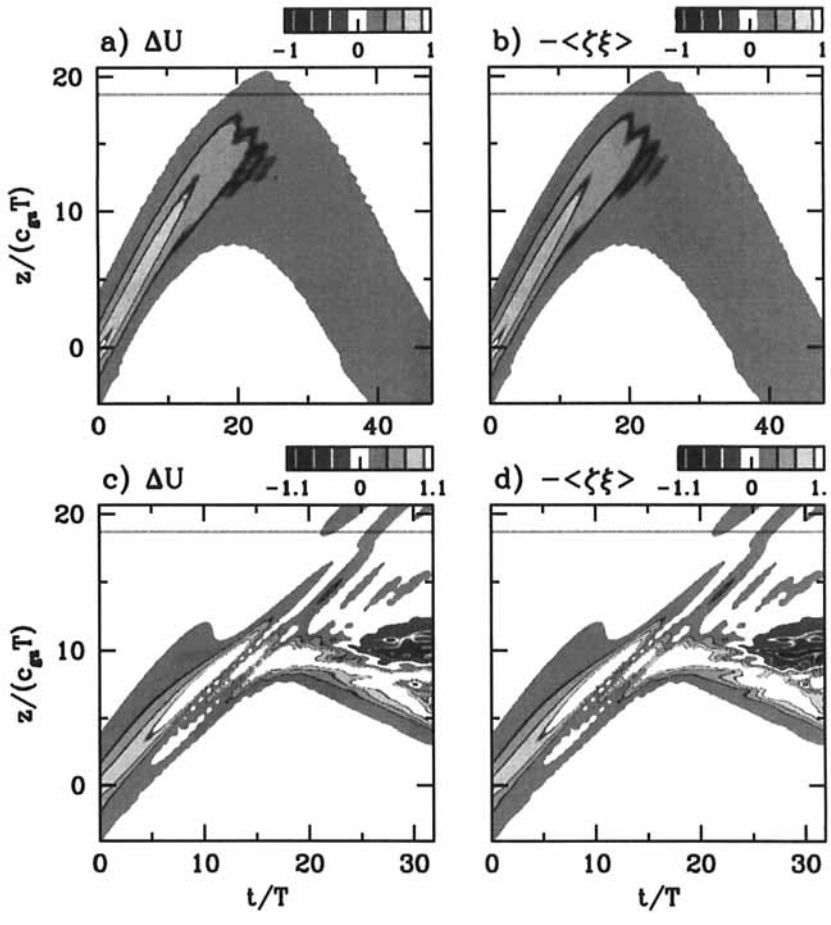

Figure 7. As in Fig. 4 but for a wave packet with $k_z = -0.7k_x$ and $A_w = 0.02N/k_x$ ((a) and (b)) and $A_w = 0.30N/k_x$ ((c) and (d)). The background shear is $s = -0.004N$. Note that the time series in (c) and (d) are shown over shorter times than in (a) and (b). See text for further details.

simulations of small- and large-amplitude wave packets. The two time series for small-amplitude waves with $A_w = -0.02N/k_x$ are shown in Figs. 4(a) and (b), respectively. As expected, the difference between the horizontally averaged flow and the initial shear flow is negligibly different from the wave-induced mean flow throughout the simulation. In the large-amplitude wave-packet simulation ($A_w = -0.30N/k_x$), the corresponding two fields in Figs. 7(c) and (d) are likewise similar, although some discrepancies appear below $z = 10c_{gz}T$ at time $t \simeq 24T$. The wave-induced mean flow is negative over a wider vertical extent than the corresponding negative region of the ΔU profile. This discrepancy continues to be enhanced at longer times (not shown) as convective instabilities develop.

Perhaps the most significant observation to be made from Fig. 7(d) is that the wave-induced mean flow increases as the wave packet reflects and it remains large for long times. Although initially the peak value is $\max(-\langle\zeta\xi\rangle) \simeq 0.08N/k_x$, at time $t \simeq 24T$ the peak value is approximately $0.12N/k_x$. This should be compared with the horizontal group velocity, $c_{gx} = \tan^2\Theta N/k_x$, where Θ is the angle to the vertical of the phase lines. During reflection the waves are approximately vertically oriented, so that

$|\Theta| \simeq 0$. Indeed, provided $|\Theta| < 19°$, the wave-induced mean flow is greater than the horizontal group velocity, and instability due to self acceleration is expected, provided these conditions persist for sufficiently long times.

Figures 5(c) and (d) show that the disturbances are overturning at time $t \simeq 22T$ (when $\Delta N^2/N^2 < -1$) and that this instability results in the efficient energy transfer to super harmonics with horizontal wave numbers $2k_x$ and $3k_x$. Higher super harmonics are also excited (not shown). Thus, in this case momentum is efficiently deposited to the mean flow through the turbulent dissipation of the disturbances. A more detailed analysis of the dissipation process was not performed since, in reality, the resulting turbulence would be fully three dimensional and could not be reproduced by the numerical model employed here. The simulations here are sufficient to demonstrate that the onset of turbulence should occur in reality.

(c) *Case:* $k_z = -1.4k_x$

In the final case discussed here, the reflection of internal waves with $k_z = -1.4k_x$ is examined. In order to properly resolve the vertical structure of these waves, these simulations were performed with twice the vertical resolution of the above two cases. The wave-packet evolution is examined in shear flow with $s = -0.016N$, this value being chosen so that the reflection level is at a height comparable to that of the two other cases discussed above.

As in Fig. 3, Fig. 8 shows time series of the momentum-flux profiles and the vertical-displacement fields of large- and small-amplitude waves. In the small-amplitude case, $A_w = 0.02N/k_x$, the wave packet reflects near $z = 15c_{gz}T$, as expected from linear theory. At early times the waves are Doppler shifted to higher frequencies as they propagate upward in the shear flow. As a result, their vertical group velocity first increases as the magnitude of the vertical wave number decreases from $|k_z| = 1.4k_x$ to $|k_z| = k_x/2^{1/2}$, and the vertical group velocity decreases as $|k_z|$ continues to decrease. In linear theory, the energy flux is proportional to the group velocity. If it is assumed that the energy associated with the waves is constant, then the energy flux should increase then decrease as the wave packet approaches the reflecting level. Likewise, the peak vertical momentum flux should increase initially as the small-amplitude waves approach the reflecting level. This is evident in Fig. 3(a) for times t up to 10 buoyancy periods. Of course, the momentum flux eventually decreases again and becomes negative when the waves reflect.

The redistribution of momentum is quite complicated in the large-amplitude case. The time series of the momentum-flux profiles is shown in Fig. 8(c) for large-amplitude waves with $A_w = 0.30N/k_x$. As in the simulations with no shear flow, (Fig. 2(f)), the initial wave packet subdivides into a train of wave packets shortly after time $t = 0$ and before reaching the reflecting level. Each component of the wave train encounters the reflecting level at different times, and at these times the momentum flux is redirected downward, resulting in a sequence of downward-propagating wave packets.

The normalized vertical displacement field at time $t \simeq 48T$, shown in Fig. 8(d), illustrates the disordered structure of the reflected waves. Below the reflecting level, super-harmonic waves and smaller-scale structures are prevalent. Surprisingly, the plot shows that a small proportion of the initial wave packet is transmitted and continues to propagate upward well above the reflecting level at this time, as indicated by the upward tilt in the phase lines at the leading edge of the wave packet.

Momentum is deposited to the mean flow as the reflecting large-amplitude waves interact, excite super-harmonic waves and dissipate, similar to the case with $k_z = -0.7k_x$.

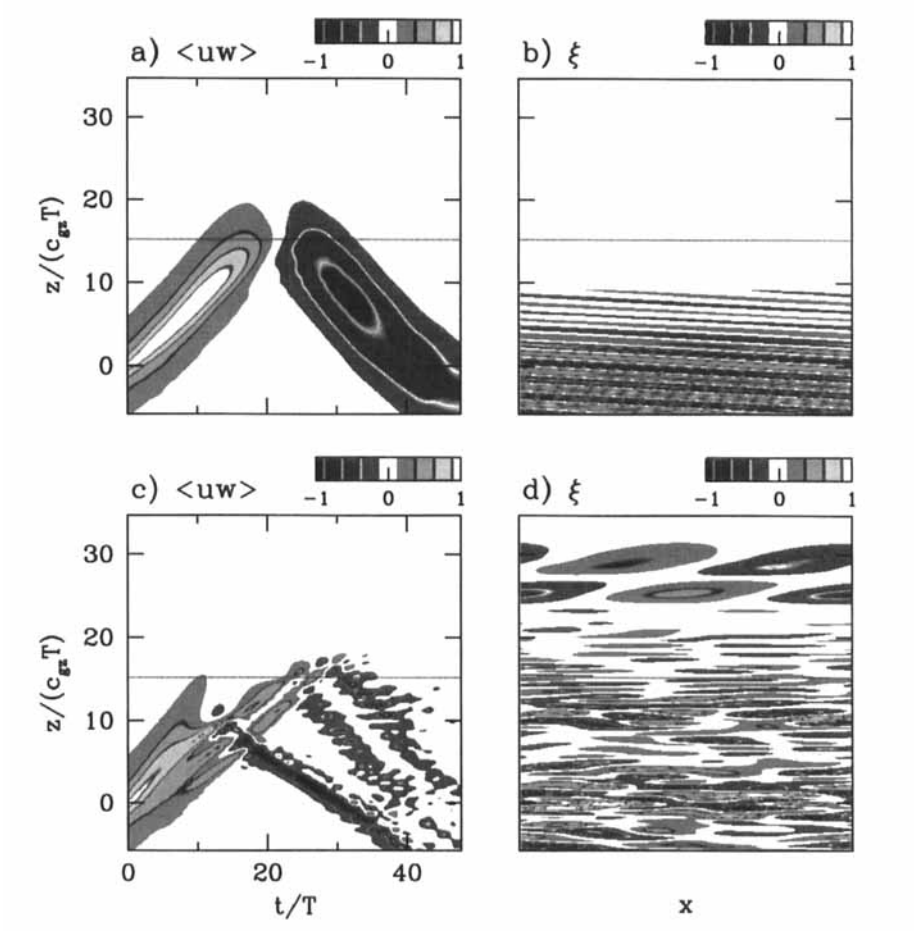

Figure 8. As in Fig. 3 but for a wave packet with $k_z = -1.4k_x$ and $A_w = 0.02N/k_x$ ((a) and (b)) and $A_w = 0.30N/k_x$ ((c) and (d)). The background shear is $s = -0.016N$. The vertical-displacement fields in (b) and (d) are shown at time $t \simeq 32T$. See text for further details.

Figures 5(e) and (f) confirm that convective instability is responsible for efficient momentum deposition. The wave-induced mean flow is positive over most of the domain when $k_z = -1.4k_x$. This is illustrated in Fig. 9, which shows times series of ΔU and $-\langle\zeta\xi\rangle$ profiles for the small- and large-amplitude simulations. Though difficult to discern from Figs. 9(c) and (d), ΔU differs from the wave-induced mean flow at late times, indicative of momentum deposition. Digitized movies of these simulations show that the flow is decelerated so that the waves below the reflecting level move backward with respect to a frame of reference moving with the horizontal phase speed of the initial upward-propagating waves.

The strength of the background shear was varied in a series of simulations to examine how the reflecting level changes for large-amplitude wave packets with $k_z = -1.4k_x$. Figure 10 shows time series of the normalized momentum-flux profiles of wave packets with $A_w = 0.30N/k_x$ and $k_z = -1.4k_x$, and with shear $s = -0.008N$ (Fig. 10(a)) and $s = -0.004N$ (Fig. 10(b)). The reflection level predicted by linear theory is indicated by the horizontal line in both plots. The two time series show that a significant fraction of the large-amplitude wave packets reflects well below the predicted

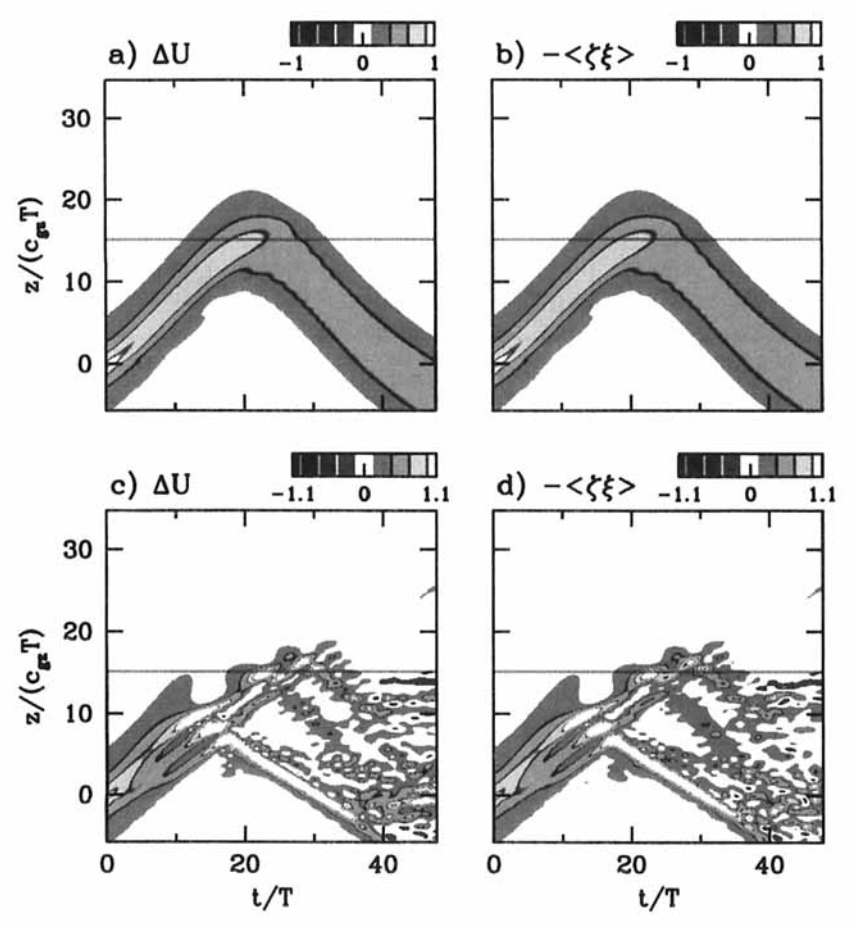

Figure 9. As in Fig. 4 but for a wave packet with $k_z = -1.4k_x$ and $A_w = 0.02N/k_x$ ((a) and (b)) and $A_w = 0.30N/k_x$ ((c) and (d)). The background shear is $s = -0.016N$. See text for further details.

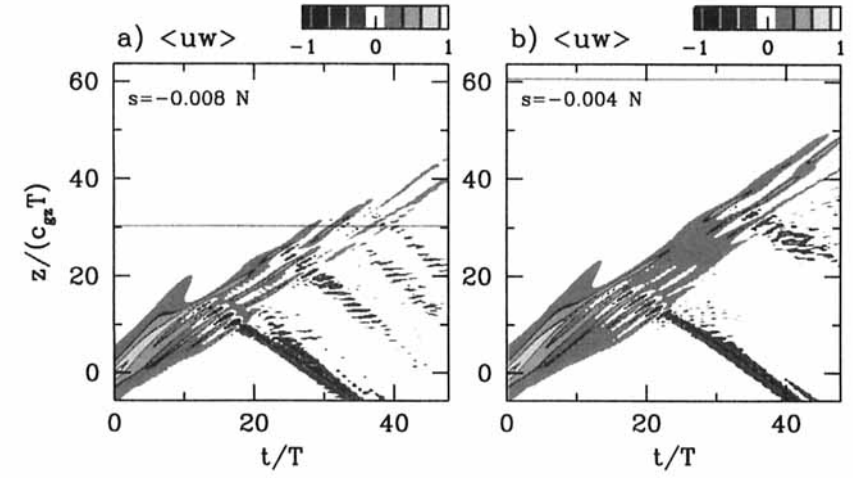

Figure 10. Time series of the normalized vertical flux of horizontal momentum per unit mass for simulations with $k_z = -1.4k_x$ and $A_w = 0.30N/k_x$. The background shear strength, s, is (a) $-0.008N$ and (b) $-0.004N$. The height of the predicted reflection level is indicated by the horizontal line. See text for further details.

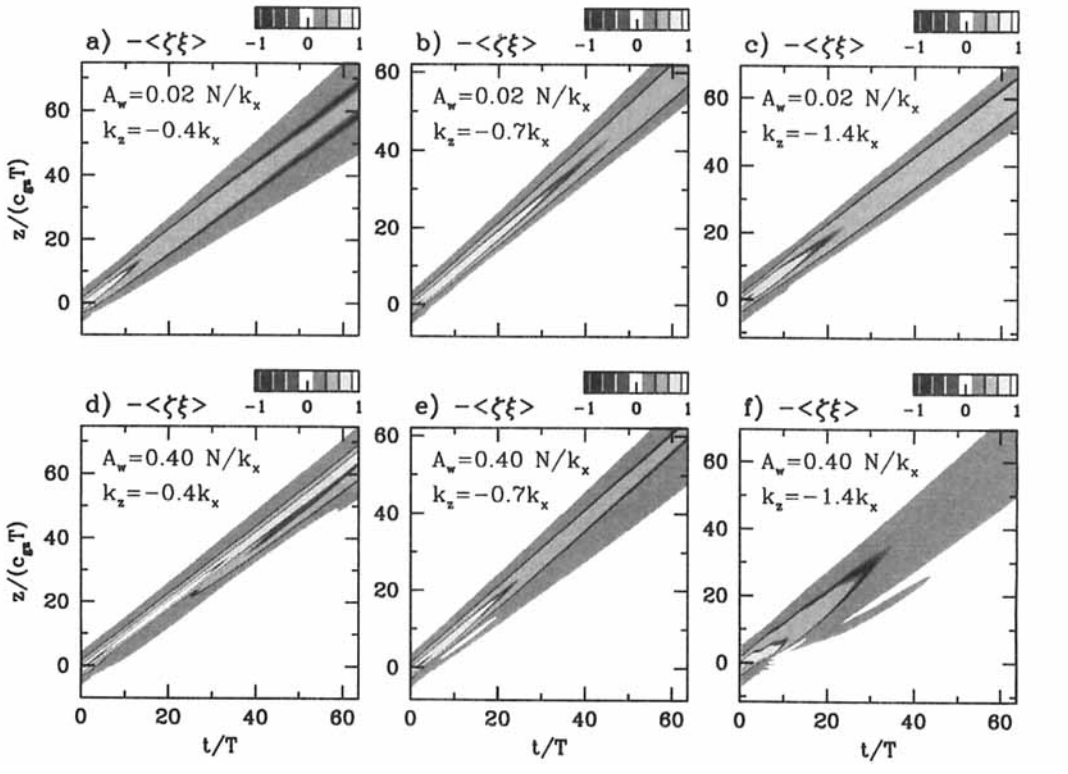

Figure 11. As in Fig. 2 but for simulations of horizontally as well as vertically compact wave packets. The initial amplitude (A_w) and vertical wave number (k_z) of the simulations are indicated on each plot. See text for further details.

reflecting level. The beam that first reflects is vertically compact, in that its extent is much smaller than the separation distance between successively reflected wave packets. Furthermore, the reflection level is a weak function of the background shear strength. Comparing Fig. 8(c) and Figs. 10(a) and (b), the first reflected beam is centred about $z = 0$ at times $t \simeq 30T$, $30T$, and $35T$ for shear strengths of $s = -0.016N$, $-0.008N$ and $-0.004N$, respectively.

5. Horizontally compact waves

Large-amplitude horizontally periodic internal waves are significantly affected by interactions between the waves and the wave-induced mean flow. However, if the wave packet is horizontally compact, the wave-induced 'mean flow' acts only over the horizontal extent of the wave packet itself. The interactions are expected to affect not only the power spectrum of the wave packet but also the horizontal structure of the wave packet itself, which is horizontally accelerated to a greater extent near the centre of the wave packet than at the left and right flanks of the wave packet, where the waves are of smaller amplitude. The effect will be pronounced if the waves are of such large amplitude that the wave-induced mean flow is comparable to the horizontal group velocity of the wave packet.

Simulations are performed on compact wave packets whose initial vertical-velocity fields are given by Eqs. (12) and (14) with horizontal and vertical extents given by $\sigma_x = 10k_x$ and $\sigma_z = 10k_x$. The nonlinear evolution of vertically and horizontally compact

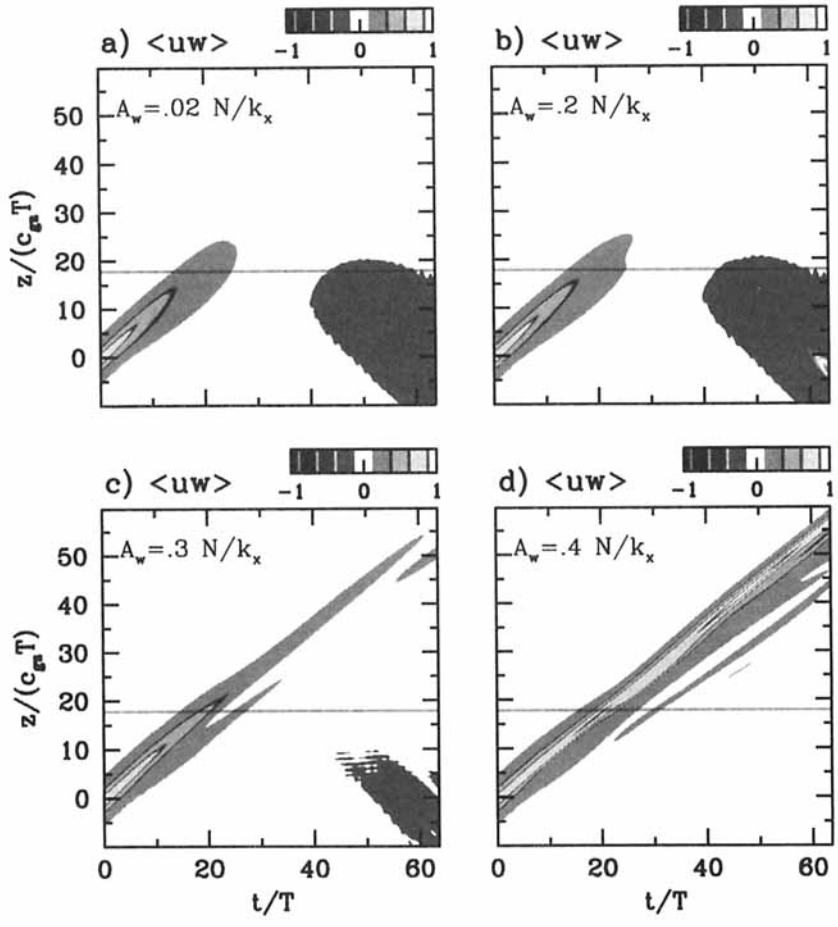

Figure 12. Time series of $\langle uw \rangle$ for simulations with $k_z = -0.4k_x$ and amplitude A_w equal to (a) $0.02N/k_x$, (b) $0.20N/k_x$, (c) $0.30N/k_x$, and (d) $0.40N/k_x$. In each simulation the background shear is $s = -0.002N$. The horizontal line on each plot indicates the predicted reflection level. See text for further details.

internal wave packets in stationary uniformly stratified fluid has been examined in detail by Sutherland (2000). In general, it is found that large-amplitude horizontally compact wave packets undergo significant horizontal dispersion, though the vertical structure does not exhibit as diverse a range in behaviour as in the horizontally periodic case.

As in Fig. 2, Fig. 11 shows time series of $-\langle \zeta \xi \rangle$, computed for simulations of small- and large-amplitude horizontally compact wave packets with $k_z = -0.4k_x$ (Figs. 11(a) and (d)), $k_z = -0.7k_x$ (Figs. 11(b) and (e)) and $k_z = -1.4k_x$ (Figs. 11(c) and (f)). Each time series is normalized by the predicted maximum initial value of $-\langle \zeta \xi \rangle$ (see Table 1).

In the small-amplitude cases, the horizontally compact and periodic waves show similar behaviour. The maximum value of $-\langle \zeta \xi \rangle$ decreases in time but only gradually in the case with $k_z = -0.7k_x$ (Fig. 11(b)). For the large-amplitude wave-packet simulation shown in Fig. 11(d), where $A_w = 0.4N/k_x$ and $k_z = -0.4k_x$, the peak value of $-\langle \zeta \xi \rangle$ initially increases over time to a maximum value at $t \simeq 20T$. Thus, the instability due to modulations of the wave packet in the vertical is still pronounced for horizontally compact wave packets. Unlike the horizontally periodic case, the wave packet continues to spread vertically over long times. In the large-amplitude cases with $k_z = -0.7k_x$

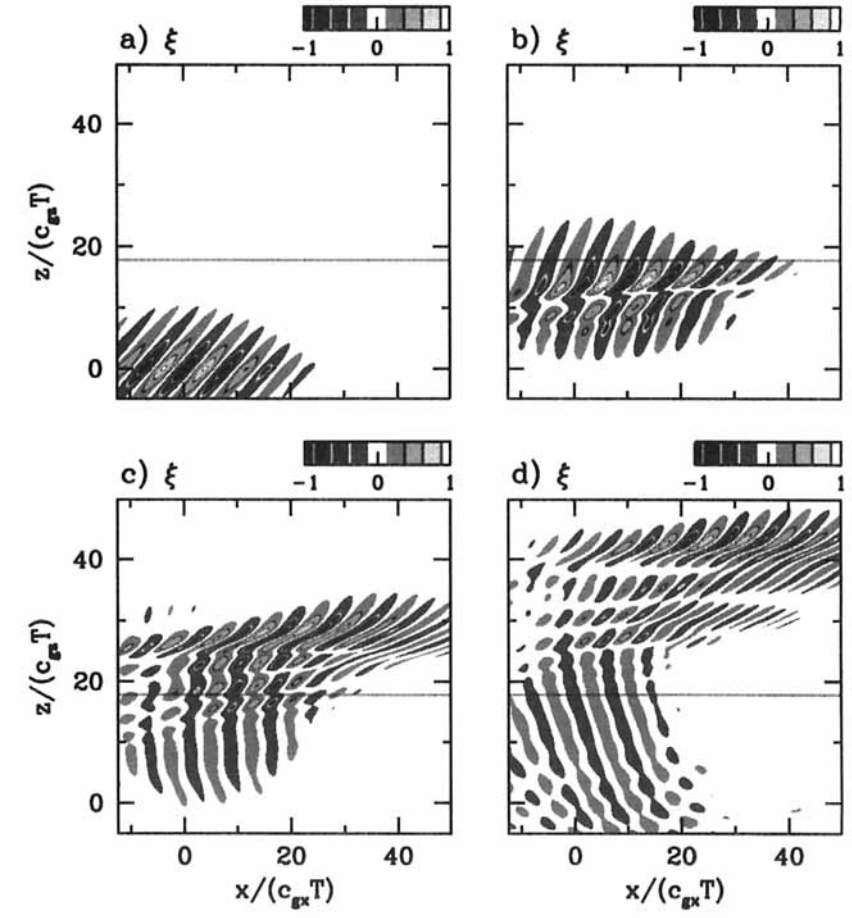

Figure 13. Vertical displacement fields at times (a) 0, (b) $\simeq 16T$, (c) $\simeq 32T$ and (d) $\simeq 48T$, shown for simulations of horizontally and vertically compact wave packets with $k_z = -0.4k_x$ and amplitude $A_w = 0.40N/k_x$. The background shear is $s = -0.002N$. The horizontal line on each plot indicates the predicted reflection level. See text for further details.

(Fig. 11(e)) and $k_z = -1.4k_x$ (Fig. 11(f)), the wave packets spread vertically rather than undergoing the weakly nonlinear modulation patterns prevalent in the horizontally periodic cases. In all three large-amplitude wave-packet simulations the waves propagate upward at a speed close to the vertical group velocity predicted by linear theory.

Despite some similarities to linear dispersion, the large-amplitude horizontally compact wave packets evolve quite differently from their small-amplitude counterparts, or from their horizontally periodic counterparts, when they encounter a reflecting level in a uniform-shear flow. As shown below, horizontally compact wave packets can transport significant momentum well beyond a reflecting level if they are of large amplitude.

(*a*) *Case:* $k_z = -0.4k_x$

Figure 12 shows time series of the normalized momentum-flux profiles for simulations of horizontally compact internal waves with vertical wave numbers $k_z = -0.4k_x$. The plots are shown for simulations of wave packets in which the normalized amplitude of the vertical-velocity field, $A_w/(N/k_x)$, is 0.02 (Fig. 13(a)), 0.20 (Fig. 13(b)),

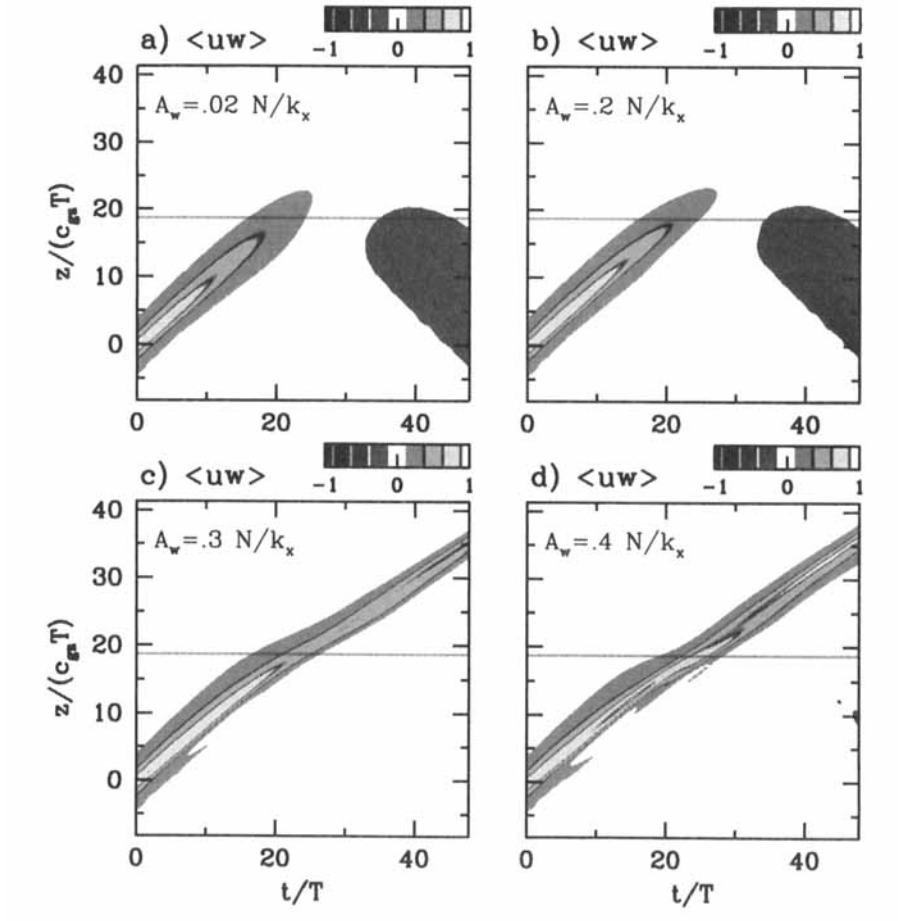

Figure 14. As in Fig. 12 but for a simulation of a wave packet with vertical wave number $k_z = -0.7k_x$ and amplitude A_w equal to (a) $0.02N/k_x$, (b) $0.20N/k_x$, (c) $0.30N/k_x$, (d) $0.40N/k_x$. In each simulation the background shear is $s = -0.004N$. See text for further details.

0.30 (Fig. 13(c)) and 0.40 (Fig. 13(d)). The obvious and surprising result of nonlinear effects is that the large-amplitude waves are capable of transporting momentum well above the reflecting level (indicated by the horizontal line in each plot). Indeed, when $A_w = 0.4N/k_x$, a negligible proportion of the wave packet is reflected downward. Simulations performed at twice the resolution give the same result.

Figure 13 shows the vertical-displacement field at times $t = 0$ (Fig. 13(a)), $\simeq 16T$ (Fig. 13(b)), $\simeq 32T$ (Fig. 13(c)), and $\simeq 48T$ (Fig. 13(d)) for a large-amplitude wave-packet simulation with $A_w = 0.4N/k_x$. The horizontal and vertical axes are normalized by the respective components of the group velocity predicted by linear theory times the buoyancy period, T. The background shear flow is prescribed so that the mean wind speed is zero at $z = 0$.

The plots show that the phase lines tilt more vertically as the wave packet approaches the reflecting level at $z \simeq 18c_{gz}T$. Shortly after time $t \simeq 16T$ the incident wave packet partially reflects generating a small-amplitude wave packet with phase lines close to the vertical below the reflecting level (Fig. 13(c)). Due to interactions between the waves and the wave-induced mean flow the phase speed of the waves decreases near

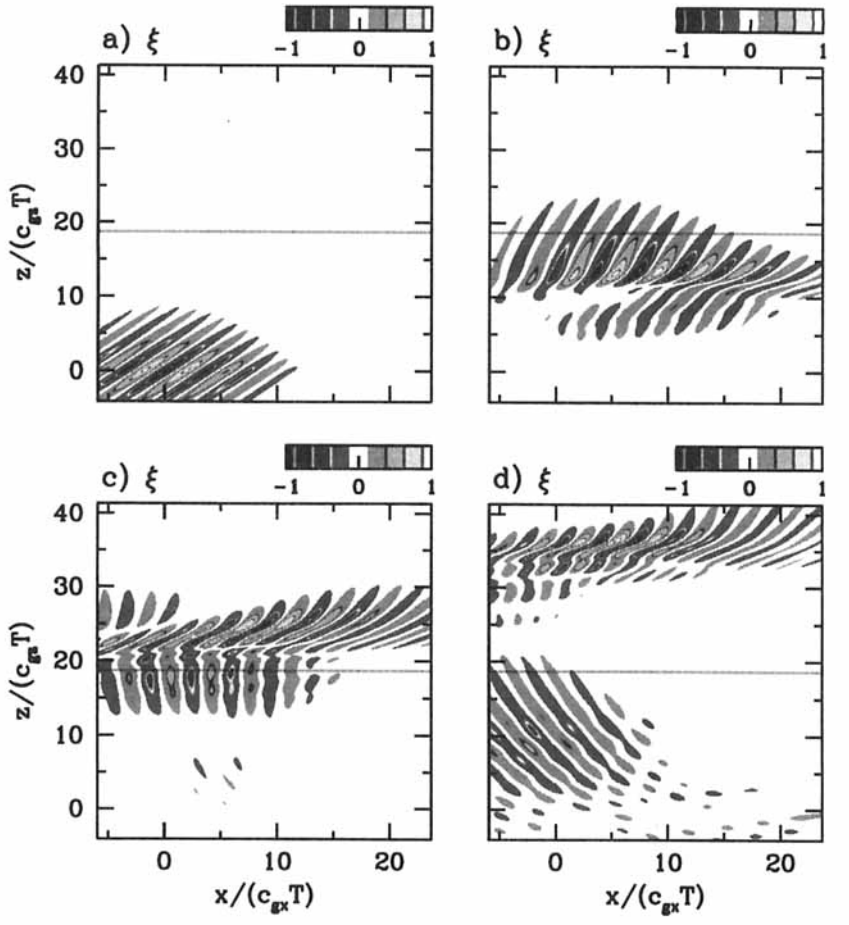

Figure 15. As in Fig. 13 but for a simulation of a wave packet with $k_z = -0.7k_x$ and $A_w = 0.40N/k_x$. The vertical-displacement fields are shown at times (a) 0, (b) $\simeq 16T$, (c) $\simeq 32T$ and (d) $\simeq 48T$. The background shear is $s = -0.004N$. See text for further details.

the reflecting level as the amplitude of the incident wave packet decreases. As a result, the phase lines of the waves above the reflecting level tilt away from the vertical. This behaviour is evident in movies constructed from successive frames of the simulation. As time progresses the leading edge of the wave packet above the reflection level maintains a similar structure and continues to propagate upward and to the right at a more-or-less constant speed (Figs. 13(c) and (d)).

Some of the properties of this transmitted wave packet appear similar to those of a solitary wave: the disturbance remains vertically localized with relatively little change in form and its structure seems to be determined by a balance between dispersion in shear flow and self focusing due to interactions between waves and the wave-induced mean flow. A detailed examination of these observations is the subject of future work.

(*b*) *Case:* $k_z = -0.7k_x$

Here, simulations are examined in which horizontally compact wave packets with different amplitudes propagate in shear flow with strength $s = -0.004N$. The vertical wave number $k_z = -0.7k_x$, close to that of small-amplitude waves with the fastest

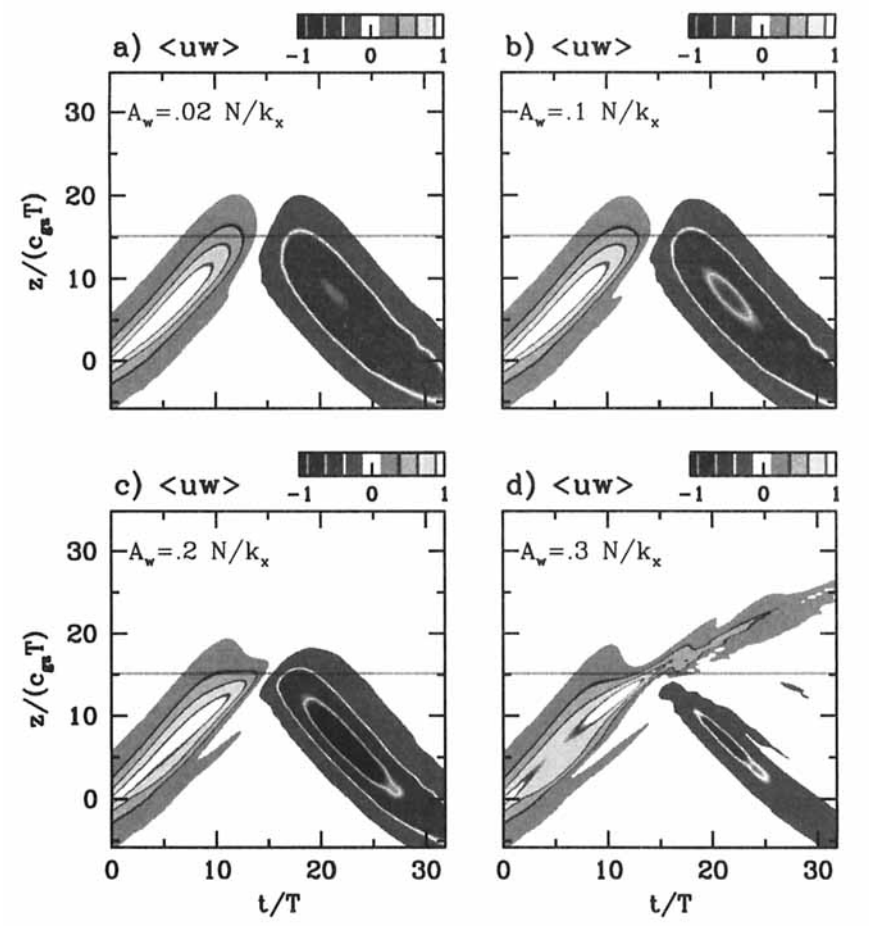

Figure 16. As in Fig. 12 but for a simulation of a wave packet with vertical wave number $k_z = -1.4k_x$ and amplitude A_w equal to (a) $0.02N/k_x$, (b) $0.10N/k_x$, (c) $0.20N/k_x$, (d) $0.30N/k_x$. In each simulation the background shear is $s = -0.016N$. See text for further details.

upward group velocity. According to linear theory, the small-amplitude waves will encounter a reflecting level near $z \simeq 18c_{gz}T$.

Similarly to the simulations with $k_z = -0.4k_x$, the large-amplitude wave packets are found to transmit well above the reflecting level if the amplitude is sufficiently large. Figure 14 shows time series of the momentum flux for four simulations of wave packets with the initial amplitude of the vertical-velocity field indicated in the upper left-hand corner of each plot. In the small-amplitude case (Fig. 14(a)) the wave packet reflects near $z \simeq 18c_{gz}T$, as anticipated from linear theory. However, the large-amplitude wave-packet simulations (Figs. 14(c) and (d)) show that relatively little momentum flux is redirected downward. Indeed, when $A_w = 0.3N/k_x$ the wave packet continues to transport momentum upward over twice the distance predicted by linear theory. The upward transport of momentum is more efficient in this case compared with wave packets with the same amplitude and $k_z = -0.4k_x$.

Figure 15 shows that a small proportion of the incident wave packet is reflected downward when $A_w = 0.4N/k_x$, although the corresponding downward momentum flux is negligible compared with the upward momentum flux associated with the wave

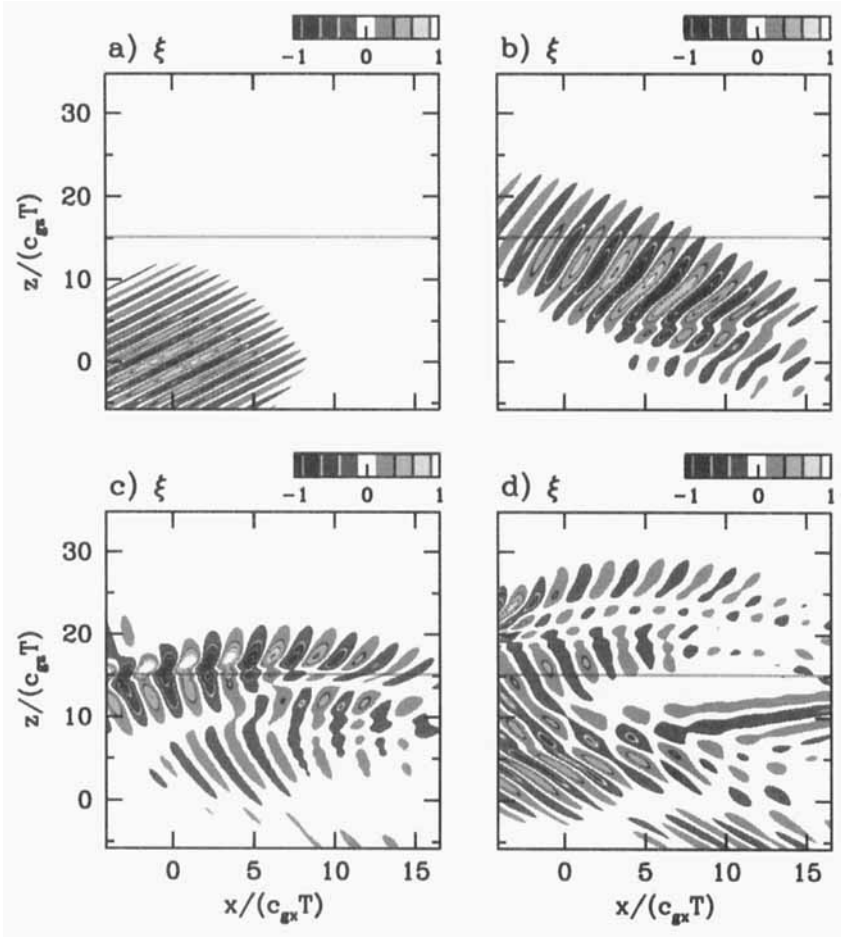

Figure 17. As in Fig. 13 but for a simulation of a wave packet with $k_z = -1.4k_x$ and $A_w = 0.30N/k_x$. The vertical-displacement fields are shown at times (a) 0, (b) $\simeq 8T$, (c) $\simeq 16T$ and (d) $\simeq 24T$. The background shear is $s = -0.016N$. See text for further details.

packet above the reflecting level (*e.g.* see Fig. 14(d)). The transmitted wave packet at time $t \simeq 48T$ (Fig. 15(d)) is more vertically localized than the initial wave packet having peak amplitude at $(x, z) \simeq (5c_{gx}T, 36c_{gz}T)$. The horizontal propagation of the wave packet is much slower than in the corresponding case with $k_z = -0.4k_x$, for which the peak amplitude occurs near $(x, z) \simeq (25c_{gx}T, 42c_{gz}T)$ after time $t \simeq 48T$.

(*c*) *Case:* $k_z = -1.4k_x$

The vertical group velocity is the smallest of the three cases examined here. The waves are examined as they propagate upward in a shear flow with $s = -0.016N$. Linear theory predicts that the reflecting level is situated near $z \simeq 15c_{gz}T$.

The time series of the momentum-flux profiles are shown in Fig. 16 for four simulations of wave packets with normalized amplitude, $A_w k_x/N$, equal to 0.02 (Fig. 16(a)), 0.1 (Fig. 16(b)), 0.2 (Fig. 16(c)), and 0.3 (Fig. 16(d)). In simulations with $A_w = 0.4N/k_x$, not shown here, the wave packet becomes convectively unstable shortly after partially reflecting at time $t \simeq 20T$.

These simulations are distinguished from those performed with lower values of $|k_z/k_x|$ in many ways. Comparing Fig. 16(c) with Figs. 12(b) and 14(b), it is found that when $k_z = -1.4k_x$, the upward momentum flux of the incident wave packet increases as it approaches the reflecting level, and the downward momentum flux of the reflected wave packet is comparable in magnitude to the incident flux at the same vertical level.

At a larger amplitude, with $A_w = 0.3N/k_x$ (Fig. 16(d)), the upward momentum flux of the incident wave packet has a sharp peak near the reflecting level between times $t \simeq 10T$ and $15T$. At later times, a significant proportion of the wave packet is found to reflect. This should be compared with the behaviour of the waves with the same amplitude but $k_z = -0.7k_x$ (Fig. 14(c)), in which a negligible proportion of the incident wave packet reflects downwards.

The effect upon the wave-packet structure of interactions between the waves and the wave-induced mean flow is shown in Fig. 17. This shows the normalized vertical-displacement field at times 0 (Fig. 17(a)), $\simeq 8T$ (Fig. 17(b)), $\simeq 16T$ (Fig. 17(c)), and $\simeq 24T$ (Fig. 17(d)). As expected from linear theory, at early times the wave packet propagates upward and to the right, its phase lines tilting more closely to the vertical as the waves propagate into ever-decreasing background mean flow speeds. Upon encountering the reflecting level, the waves are partially transmitted and reflected, and the horizontal group velocity of the two wave packets decreases. Indeed, at late times the two wave packets translate from right to left.

6. Discussion and conclusions

The simulations show that horizontally periodic internal waves can deposit momentum near a reflecting level if the amplitude of the incident waves is sufficiently large. A criterion predicting when momentum deposition occurs is estimated from the self-acceleration condition, Eq. (10) (which determines the maximum amplitude of vertically compact wave packets propagating in stationary uniformly stratified fluid), and is given by Eq. (11). Some values of this critical amplitude are listed in Table 2.

For example, in the case with $k_z = -0.4k_x$, momentum deposition is expected if $A_w k_x/N > 0.23$. This is consistent with the results shown in Fig. 4. Likewise, in simulations with $k_z = -0.7k_x$ and $-1.4k_x$ momentum is found to be deposited to the mean flow when the amplitude of the initial wave packet exceeds the critical value predicted by Eq. (11).

For the purposes of improving the parametrization of momentum deposition by large-amplitude internal waves, it would be desirable to quantify this work further by determining the partitioning of momentum transport and deposition by a large-amplitude wave packet incident on a reflecting level. However, because the breaking process must involve three-dimensional behaviour, which is prohibited in the simulations performed here, it would be misleading to provide such an estimate based on these simulations. A comprehensive study of the fully three-dimensional dynamics has been initiated to provide a more realistic assessment of the internal wave dynamics near a reflecting level.

Of course, if the incident wave packet is horizontally as well as vertically compact, one does not expect that the waves, even at large amplitude, could accelerate the mean flow across the entire domain. Wave breaking would affect the time-mean motions only over the horizontal extent of the wave packet. Indeed, simulations show that the wave packet does not break at all when it is horizontally compact. Instead, particularly for wave packets with phase tilt, Θ, close to zero, a substantial proportion of the large-amplitude wave packet is found to propagate well above the reflecting level.

The enhanced transmission of a large-amplitude wave packet across a reflecting level has been observed previously by Sutherland (1999), who studied the propagation of compact wave packets across a hyperbolic tangent shear layer (with constant velocity well above and well below the reflecting level). That study showed that interactions between the waves and the wave-induced mean flow acted to decrease the intrinsic frequency of the transmitted wave packet. If the amplitude of the incident wave packet was so large that the resulting intrinsic frequency beyond the reflecting level was smaller than the background buoyancy frequency, then the transmitted wave packet could propagate indefinitely.

In this case, the background flow is constant shear. This means that, even though a large-amplitude wave packet could be transmitted across a reflecting level as argued above, the resulting wave packet must ultimately encounter another reflecting level further up. The wave packet should not propagate upward indefinitely.

The simulations here do not bear out this hypothesis.

As Figs. 12 and 14 illustrate, if the incident wave packet is horizontally compact, with $|k_z/k_x| < 1$, and if it is of sufficiently large amplitude, then the momentum flux is transported vertically upward at a nearly constant rate well above the reflecting level. The structure of the transmitted wave packet does not change shape significantly as it continues to propagate upward. It appears as though the transmitted wave packet propagates in a quasi-steady state. Resolution-doubling tests were performed to confirm that this behaviour is not an artefact of the numerical model.

One might attempt to explain this behaviour by arguing that a steady state might be reached if the shear associated with the wave-induced mean flow is comparable in magnitude (but opposite in sign) to the background shear. From linear theory, a quantitative estimate can be formulated to determine the minimum amplitude of the incident wave packet necessary for the generation of a steady-state transmitted wave packet. In terms of the maximum amplitude, A_w, of the vertical-velocity field, the maximum shear associated with the wave-induced mean flow is

$$\max\left\{\frac{\mathrm{d}}{\mathrm{d}z}(-\langle\xi\zeta\rangle)\right\} = (A_w k_x/N)^2 \frac{1}{2}\frac{N}{k_x\sigma_z}\frac{1}{\cos^3\Theta}. \tag{15}$$

Following the above argument, it is assumed that a steady-state transmitted wave packet may be generated if the amplitude of the initial wave packet is sufficiently large that the wave-induced shear flow given by Eq. (15) is at least as great as the background shear, s. Comparing and re-arranging gives a condition for the critical amplitude:

$$A_w^{\text{transmit}} \simeq \left(2\sigma_z k_x \frac{s}{N}\cos^3\Theta\right)^{1/2} N/k_x. \tag{16}$$

Table 2 lists some values of the critical amplitude for the steady-state transmission of horizontally compact waves given by Eq. (16). The critical breaking amplitude is greater than the critical amplitude for transmission in simulations with $k_z = -0.4k_x$ and $-0.7k_x$. Indeed, it is these two simulations that clearly show quasi steady-state transmission for amplitudes $A_w \geq 0.3N/k_x$. In the case with $k_z = -1.4k_x$, the critical breaking amplitude is less than the transmission amplitude explaining why weaker transmission occurs in simulations of waves with amplitude $A_w \geq 0.3N/k_x$.

In general, these simulations show that the behaviour of large-amplitude nonhydrostatic internal waves (for which $|k_z/k_x| < 1$) deviates significantly from that predicted by linear theory. The redistribution of momentum by reflecting and breaking waves has yet to be accurately determined in fully three-dimensional numerical simulations. Nonetheless, the issues raised here illustrate the dynamics of two important processes

that must ultimately be considered when attempting to parametrize the effect of drag on the atmosphere by nonhydrostatic internal waves: a reflection level may not pose such a barrier to nonhydrostatic wave propagation as previously supposed; and waves may break not only near a critical level but also near a reflection level.

ACKNOWLEDGEMENTS

This work has been supported, in part, by funding from the Natural Sciences and Engineering Research Council of Canada.

REFERENCES

Benielli, D. and Sommeria, J. 1996 Excitation of internal waves and stratified turbulence by parametric instability. *Dyn. Atmos. Oceans*, **23,** 335–343

1998 Excitation and breaking of internal gravity waves by parametric instability. *J. Fluid Mech.*, **374,** 117–144

Benjamin, T. B. and Feir, J. E. 1967 The disintegration of wavetrains on deep water. *J. Fluid Mech.*, **27,** 417–430

Booker, J. R. and Bretherton, F. P. 1967 The critical layer for internal gravity waves in shear flow. *J. Fluid Mech.*, **27,** 513–539

Bouruet-Aubertot, P., Sommeria, J. and Staquet, C. 1995 Instabilities and breaking of standing internal gravity waves. *J. Fluid Mech.*, **285,** 265–301

1996 Stratified turbulence produced by internal wave breaking: Two-dimensional numerical experiments. *Dyn. Atmos. Oceans*, **23,** 357–369

Bretherton, F. P. 1966 Gravity waves in shear. *Q. J. R. Meteorol. Soc.*, **92,** 466–480

1969 Momentum transport by gravity waves. *Q. J. R. Meteorol. Soc.*, **95(404),** 213–243

Broad, A. S. 1995 Linear theory of momentum fluxes in 3-D flows with turning of the mean wind with height. *Q. J. R. Meteorol. Soc.*, **121,** 1891–1902

1999 Do orographic gravity waves break in flows with uniform wind direction turning with height? *Q. J. R. Meteorol. Soc.*, **125,** 1695–1714

Drazin, P. G. 1977 On the instability of an internal gravity wave. *Proc. R. Soc. London*, **356,** 411–432

Fermi, E., Pasta, J. and Ulam, S. 1974 'Studies of nonlinear problems I', Los Alamos Report LA 1940, 1955. Reproduced in *Nonlinear Wave Motion*. Ed. A. C. Newell. Am. Math. Soc., Providence, RI, USA

Fritts, D. C. and Dunkerton, T. J. 1984 A quasi-linear study of gravity-wave saturation and self-acceleration. *J. Atmos. Sci.*, **41,** 3272–3289

Gill, A. E. 1982 *Atmosphere–ocean dynamics*. Academic Press, San Diego, USA

Grimshaw, R. H. J. 1977 The modulation of an internal gravity-wave packet, and the resonance with the mean motion. *Studies Appl. Math.*, **56,** 241–266

Hasselmann, K. 1967 A criterion for non-linear wave stability. *J. Fluid Mech.*, **30,** 737–739

Klostermeyer, J. 1991 Two- and three-dimensional parametric instabilities in finite amplitude internal gravity waves. *Geophys. Astrophys. Fluid Dyn.*, **64,** 1–25

Lighthill, M. J. 1978 *Waves in fluids*. Cambridge University Press, Cambridge, UK

Lindzen, R. S. 1981 Turbulence and stress owing to gravity wave and tidal breakdown. *J. Geophys. Res.*, **86,** 9707–9714

Lombard, P. N. and Riley, J. J. 1996 On the breakdown into turbulence of propagating internal waves. *Dyn. Atmos. Ocean*, **23,** 345–355

McIntyre, M. E. 1973 Mean motions and impulse of a guided internal gravity wave packet. *J. Fluid Mech.*, **60,** 801–811

Mied, R. R. 1976 The occurrence of parametric instabilities in finite-amplitude internal gravity waves. *J. Fluid Mech.*, **78,** 763–784

Phillips, O. M. 1960 On the dynamics of unsteady gravity waves of finite amplitude. Part 1. The elementary interactions. *J. Fluid Mech.*, **9,** 193–217

1981 Wave interactions—the evolution of an idea. *J. Fluid Mech.*, **106,** 215–227

Shutts, G. J.	1995	Gravity-wave drag parametrization over complex terrain: The effect of critical level absorption in directional wind shear. *Q. J. R. Meteorol. Soc.*, **121,** 1005–1021
	1998	Stationary gravity-wave structure in flows with directional wind shear. *Q. J. R. Meteorol. Soc.*, **124,** 1421–1442
Sutherland, B. R.	1996	Internal gravity wave radiation into weakly stratified fluid. *Phys. Fluids*, **8,** 430–441
	1999	Propagation and reflection of large amplitude internal gravity waves. *Phys. Fluids*, **11,** 1081–1090
	2000	Finite-amplitude internal wavepacket dispersion and breaking. *J. Fluid Mech.*, in press
Sutherland, B. R. and Linden, P. F.	1998	Internal wave generation by flow over a thin barrier. *J. Fluid Mech.*, **377,** 223–252
Whitham, G. B.	1965	A general approach to linear and nonlinear dispersive waves using a Lagrangian. *J. Fluid. Mech.*, **22,** 273–283
	1974	*Linear and nonlinear waves.* John Wiley and Sons, Inc., New York, USA